Immunopathology and parasite sequestration cause severe cerebral trypanosomiasis in animals

Sara Silva Pereira
Instituto de Medicina Molecular Joao Lobo Antunes https://orcid.org/0000-0002-6590-6626
Mariana De Niz
Instituto de Medicina Molecular Joao Lobo Antunes https://orcid.org/0000-0001-6987-6789
Karine Serre
Instituto de Medicina Molecular Joao Lobo Antunes https://orcid.org/0000-0001-9152-4739
Marie Ouarné
Instituto de Medicina Molecular Joao Lobo Antunes https://orcid.org/0000-0003-4724-4363
Claudio A Franco
Instituto de Medicina Molecular Joao Lobo Antunes https://orcid.org/0000-0002-2861-3883
Luisa M Figueiredo (figueiredolm@gmail.com)
Instituto de Medicina Molecular Joao Lobo Antunes https://orcid.org/0000-0002-5752-6586

Research Article

Keywords: cerebral trypanosomiasis, sequestration, Trypanosoma congolense, animal African trypanosomiasis, disease severity, immunopathology

Posted Date: November 5th, 2021

DOI: https://doi.org/10.21203/rs.3.rs-1050698/v1

Abstract

Trypanosoma congolense causes a syndrome of variable severity in animals in sub-Saharan Africa. Cerebral trypanosomiasis is an acute form, but the mechanism underlying this severity remains unknown. We developed a mouse model of cerebral trypanosomiasis with *T. congolense* strain 1/148 and characterized the cellular, behavioral and physiological consequences of this infection. Using *in vivo* imaging, we show large parasite sequestration in the brain vasculature for long periods of time (up to 8 hours), that results in extensive brain damage partly caused by ICAM1-mediated recruitment and accumulation of T cells. Antibody-mediated ICAM1 blocking and lymphocyte absence reduce parasite sequestration in the brain and prevent the onset of cerebral trypanosomiasis. Here, we establish a new mouse model of cerebral trypanosomiasis and we propose a mechanism whereby parasite sequestration, host ICAM1, and T cells play a pivotal role.

Introduction

Endothelial sequestration enables pathogen cytoadhesion to the blood vasculature and is key for survival of certain parasites and bacteria in their mammalian hosts. *Trypanosoma congolense*, the most prevalent and pathogenic African trypanosome species in African livestock (van den Bossche et al., 2011), is a fully intravascular parasite that employs sequestration by cytoadhering to the endothelial cells of several mammals (Banks, 1978; Hemphill et al., 1994).

Understanding the molecular basis of animal African trypanosomiasis (AAT) disease severity is of foremost importance because natural infections display wide variability in pathogenesis and clinical outcome. Disease can be acute with ≤70% mortality per herd, or chronic; and signalment can range from mild fever, anemia, and weight loss, to cachexia, acute inflammatory syndrome, disseminated intravascular coagulation syndrome, and neurological impairment, that ultimately culminate in generalized organ failure and death. Animals can experience necrotic and hemorrhagic lesions in major organs, particularly the brain, liver, and spleen (Silva Pereira et al., 2019), but can also remain chronically infected with less severe signalment, or be asymptomatic (Berthier et al., 2015; Mamoudou et al., 2016). The reasons behind such large phenotypic variability are unknown, but we hypothesize that differential parasite sequestration plays an important role. This has been observed in other parasitic infections, such as *Plasmodium falciparum*, the causative agent of malaria, where sequestration is directly linked to disease severity, by causing cerebral malaria when happening in the brain (Ghazanfari et al., 2018), malaria-associated acute respiratory distress syndrome when in the lungs (Van den Steen et al., 2013), or placental malaria when in the placenta (Rogerson et al., 2007).

Parasite sequestration usually results in an inflammatory response (Storm and Craig, 2014). We know that *T. congolense* cytoadhesion to host cell membranes triggers antibody-complement cascades and increases vascular permeability, suggestive of endothelium damage (Banks, 1980). The parasite itself has also been reported to release soluble molecules, like trans-sialidades, that activate the endothelium,

enhancing inflammation (Ammar et al., 2013). It is therefore plausible that the physical damage caused by parasite cytoadhesion and the resulting host's immune response affect disease progression.

Here, we report the first mouse model of cerebral trypanosomiasis in animals and investigate its disease mechanism in living animals. We characterized parasite distribution in the mouse vasculature, vessel diameter preference, and duration of parasite-endothelial cell interaction. Furthermore, we assessed the impact of infection on the brain endothelium and on the onset of cerebral trypanosomiasis. Our data showed that cerebral trypanosomiasis is caused by a combination of increased parasite sequestration in the brain and T cell activation, via upregulation of intercellular adhesion molecule 1 (ICAM1) expression in both endothelial and circulating myeloid cells. These findings highlight the importance of parasite sequestration and provide a cellular mechanism for the development of cerebral trypanosomiasis in animals.

Results

A virulent strain of T. congolense causes cerebral trypanosomiasis

To investigate the basis of disease severity caused by *T. congolense*, we used two parasite strains of different virulence. Infection of C57BL/6J mice with strain 1/148 resulted in acute disease with mean mouse survival of 9.0±0.4 days (N = 4) (Figure 1A). The majority of mice did not survive beyond the first peak of parasitaemia (Figure 1B). Within one to three days to the time of death, mice showed growing signs of neurological impairment, including loss of proprioception, hemiparesis (i.e. weakness in one side of the body), and strength and grip loss in the limbs. In contrast, infections with strain IL3000 resulted in 3-5 defined peaks of parasitaemia (Figure 1B). These mice died within 77.5±4.0 days (Figure 1A) with multi-systemic pathology.

We compared organ pathology at the first peak of parasitaemia and observed that infection with strain 1/148 resulted in marked damage to the brain, kidney, and thymus; moderate damage in the liver; and mild damage to the heart, lungs, and spleen (Figure 1C). Infection with strain IL3000 resulted also in moderate damage to the liver, but only mild damage to the spleen, thymus and testes, and minimal to the heart (Figure 1C). Importantly, whilst there were no pathological changes in the brain of mice infected with IL3000, 1/148 infections resulted in large brain lesions characterized by multifocal grey matter vacuolation, ischemia, neuronal loss and hemorrhages (Figure 1D), which were the most likely cause of death. Parasite labelling by immunohistochemistry showed large parasite accumulation in the brain vasculature (Figure 1E), to the point of vascular occlusion in smaller capillaries. Parasite accumulation in the brain vasculature during natural infections has been described in the literature, including in cattle, dogs, horses, and wild animals, some of which have been reported to develop neurological impairment (Losos and Gwamaka, 1973; Losos and Ikede, 1972; Losos et al., 1971; Savage et al., 2021).

The proportion of Trypanosoma congolense sequestration varies with strain and tissue, independently of parasite load

Given the severity of lesions in the host and the large accumulation of parasites in the brains of animals infected with the *T. congolense* strain 1/148, we hypothesized that early death was caused by parasite sequestration in the brain vasculature. Cytoadhesion and sequestration are often used interchangeably. Here, we refer to cytoadhesion as the physical act of parasite binding to the endothelium, and to sequestration as the mechanism.

Therefore, we started by confirming that *T. congolense* parasites cytoadhered to the endothelium by intravital microscopy. Since we did not have access to fluorescent 1/148 parasites, we used FITC-Dextran and Hoechst dye to visualize the intravascular environment and the nuclei of circulating cells, respectively (Figure 2A), as well as α-A637-CD31 to mark the vascular endothelium (Figure 2B). This combination of markers allowed us to quantify parasites in vessels. Then, based on parasite mobility during live imaging, we compared total parasite load and the percentage of cytoadhered parasites in major organs in the first 6 days of 1/148 infection and at three points in IL3000 infection (first peak, second peak, and post-second peak). For representative image acquisition, we perfused mice to remove free-flowing parasites (i.e. not cytoadhered) (Figure 2B). In 1/148 infections, total parasite load increased linearly with time in the brain (R^2 = 0.83, Pearson's correlation) and adipose tissue (R^2 = 0.68, Pearson's correlation) (Figure 2C, left). In remaining organs, parasite load oscillated during infection. For instance, in the liver, parasite load was maximal already on day 2; in the spleen, maximum parasite load was reached on day 5 p.i; and in the lungs on day 4 p.i.. The brain was the organ with the highest parasite load at day 6 p.i., and variability across replicates was low (Figure 2C and 2D, left, Video S1). This was also the maximum parasite load registered throughout the course of infection amongst all organs. In IL3000 infections, parasite load was highest in the lungs, at both peaks of parasitaemia (1.25 to 8.64 x 10^5 parasites / cm^2 vessel), followed by heart (1.14 to 2.15 x 10^5 parasites / cm^2 vessel) and brain (0.61 to 2.16 x 10^5 parasites / cm^2 vessel). Parasite distribution from the first to second peaks of parasitaemia did not change drastically, but there was a 2-fold decrease in the spleen (Figure 2C, right). After the second peak of parasitaemia, in a window of undetectable peripheral parasitaemia by hemocytometry, there was a small number of parasites detectable in the brain, heart, lungs, pancreas, and spleen. An example of a parasite cytoadhered to the endothelium of a pancreatic arteriole can be seen in Video S2.

Unexpectedly, parasite sequestration did not increase linearly with parasite load in neither 1/148 nor IL3000 infections (Figure 2E). For all organs, parasites began sequestering at day 1 p.i., but throughout infection the percentage of cytoadhered parasites oscillated in an organ-dependent manner. In 1/148 infections, in the brain and pancreas, parasite sequestration was maximal at day 6 p.i. and the proportion of sequestered parasites (over the total number of parasites recorded) was higher than 80%. In remaining organs, the percentage of parasite sequestration was highest earlier in infection (Figure 2E and 2F, left). In IL3000 infections, parasite sequestration at the first peak of parasitaemia was highest in the kidney and spleen (all detected parasites were cytoadhered), followed by the heart (92% ± 3, respectively) (Figure 2E and 2F, right). During the second peak of parasitaemia, sequestration was lowest in the lungs (11% ± 3, compared to 75% ± 3 in the first peak), and highest in the kidney (85% ± 4). After the second peak, and despite the above-mentioned low parasite load, all parasites in the spleen and lungs and 92% ± 6 in the

heart were cytoadhered, suggesting that these sequestered parasites escaped immune or splenic clearance. Representative images of *T. congolense* sequestration in the different organs at the first peak of parasitaemia (day 6 p.i. for 1/148 and days 7-10 p.i. for IL3000 infections) are shown in Figure S1.

Together, these data showed that parasite sequestration is tissue-, strain- and time-dependent, but not a consequence of high parasitaemia. Importantly, given that the brain was the organ with the highest parasite load and the highest sequestration at day 6 after 1/148 infection, it supported the hypothesis that parasite sequestration contributed to cerebral trypanosomiasis and early death.

Individual parasites sequester in the brain vasculature for up to 8 hours

We sought to investigate how tropism is established by parasites of strain 1/148 preferentially sequestering in the brain. Therefore, we used ex-vivo microscopy to understand whether they accumulated in particular brain regions or brain vessels. Mice were infected and, at day 6 post-infection, brains were surgically removed, dissected into ten anatomical regions, and imaged immediately. We found that, in both 1/148 and IL3000 infections, parasites accumulated in the posterior parts of the brain (i.e. cerebellum, midbrain, pons, medulla) (Figures 3A and 3B, left). However, while IL3000 sequestration reproduced this pattern, 1/148 sequestration was evenly distributed across vessels of all brain sections (Figures 3A and 3B, right). Next, we questioned whether vessel caliber was a determinant of parasite sequestration, so we compared the number of parasites in capillaries ($\varphi < 10$ µm), and arterioles/venules of different diameters ($10 \leq \varphi > 20$ µm, $20 \leq \varphi > 40$ µm, $\varphi \geq 40$ µm). We found that *T. congolense* parasites distributed evenly (Figure 3C, left) and sequestered in similar proportions throughout vessels of all diameters (Figure 3C, right).

We observed that *T. congolense* parasites can adhere to the brain endothelium with every part of their cell (Figure 3D), including the cell body (Video S3), the posterior end (Video S4), the distal flagellum (Video S5), or a mixture (i.e. when during the duration of the video parasites attached with more than one part of their cell). IL3000 parasites adhered less with the posterior end and more with the distal flagellum than 1/148 parasites (10% ± 6 *vs.* 24% ± 5 and 45% ± 5 *vs.* 32% ± 7, respectively; $p < 0.001$, unpaired t-test) (Figure 3E). We then followed 100 parasites for up to 10 hours and discovered that 1/148 parasites remained cytoadhered to the same endothelial cell for longer than IL3000 and to a maximum of 8 hours (median of 2 hours ± 7 minutes and 5 hours ± 11 minutes for IL3000 and 1/148, respectively) (Figure 3F).

In summary, we observed that parasites of both strains preferentially colonized the vasculature of the posterior parts of the brain, but that 1/148 cytoadhered equally well across brain regions, corroborating our earlier observation that sequestration was independent of parasite load. These experiments also showed very little physical constraints for parasite distribution and sequestration, as parasites distributed and cytoadhered to vessels of all calibers and interacted with the endothelium using any part of their bodies. Importantly, we showed that 1/148 sequestration in the brain is a longer-lived interaction, thus corroborating the tropism of this strain to the brain vasculature.

These observations, together with the fact that *T. congolense* 1/148 infections result in shorter mouse survival, significant neuropathology, and increased parasite sequestration in the brain, indicate that *T. congolense* 1/148 infection in C57BL6/J mice are a good model of cerebral trypanosomiasis. For the remaining of this study, we investigated the mechanism behind cerebral trypanosomiasis in mice.

T. congolense **1/148 infection induces a pro-inflammatory profile in brain endothelial cells**

We started by characterizing how the brain endothelium responded to 1/148 infection. To achieve this, we infected RiboTag.PDGFb-iCRE mice, which, upon induction of Cre recombinase activity, express a hemagglutinin tag at the ribosomes of the endothelial cells. We harvested the brain, captured the polysomes of the endothelial cells by immunoprecipitation, and sequenced the mRNA that was in translation (Sanz et al., 2009) (Figure 4A). We compared the expression profiles of brain endothelial cells of mice non-infected and infected with *T. congolense* 1/148 and found that infection resulted in downregulation of 588 genes and upregulation of 612 genes (Figure 4B and Table S1).

Within the 20 most downregulated genes, we found a variety of functions, including genes involved in metabolism, efflux transport, and two genes involved in maturation of B cells (lymphocyte antigen 6 complex, locus C1 (Ly6c1) and tumor necrosis factor receptor superfamily, member 17 (Tnfrsf17m also called BCMA)) (Figure 4C). Within the 20 most upregulated transcripts, we detected several genes involved in the immune response, and in particular those related to type 1 immunity and interferon-dependent pathways (i.e. CXCL10, CXCL9, Basic leucine zipper transcription factor (Batf2), Growth differentiation factor 15 (Gdf15), CD300-like family member F (CD300lf), Z-DNA binding protein 1 (Zbp1), and guanylate-binding protein 10 (Gbp10). We also detected transcripts involved in angiogenesis, endothelial transmigration, and in the response to blood-brain-barrier dysfunction, including amyloid precursor protein (APP), stanniocalcin 1 (Stc1), serine peptidase inhibitor (Serpina3f), syntenin 2 (Sdcbp2), angiopoietin 2 (Angpt2), and placental growth factor (Pgf) (Figure 4C).

To study the predicted biological function of upregulated genes in a more systematic and unbiased way, we performed gene set enrichment analysis of the 612 genes (GSEA) (Table S2). Results were consistent with the signature we observed from the most upregulated genes, as 63% of the enriched gene sets related to inflammatory responses (e.g. response to interferon gamma, positive regulation of defense response, response to tumor necrosis factor, cytokine-mediated signaling pathway, regulation of innate immune response, response to virus, response to interleukin-1, antigen processing and presentation, regulation of inflammatory response, leukocyte migration, etc.), and 7% to angiogenesis (e.g. angiogenesis, regeneration) (Figure 4D).

Given that the transcriptomic analysis revealed signs of a strong pro-inflammatory response, we asked if the serum cytokine levels were consistent with such response. For that, at days 3 and 6 p.i., we assessed the serum levels of six cytokines present either in the 20 most upregulated genes or the enriched gene sets (i.e. IL-1α, IL-1β, IFNγ, CXCL10, CXCL9, TNFα). We confirmed a significant increase in the levels of IFNγ at day 3 p.i. ($\log_2$ FC = 2.82) (2-way ANOVA, *p*-value = 0.01), an increase in CXCL10 at day 6 p.i. ($\log_2$

FC = 2.53) (2-way ANOVA, *p*-value = 0.01), and an increase in CXCL9 at both days 3 and 6 p.i. compared to the non-infected control ($\log_2$ FC = 3.45 and 4.30, respectively) (2-way ANOVA, *p*-value = 0.03 and 0.002, respectively) (Figure 4E). These results support the presence of a systemic pro-inflammatory response in the first week of infection with 1/148 strain.

Given that an activated endothelium upregulates the expression of integrins which control the immune response, we also assessed the expression changes of intercellular adhesion molecule (ICAM) 1, ICAM2, and vascular cell adhesion molecule (VCAM) 1, three integrins involved in leukocyte transendothelial migration. We compared expression of ICAM1, ICAM2, and VCAM1 proteins in the vasculature of the brain at day 6 p.i., by ex-vivo microscopy (Figure 4F). Consistent with the endothelium ribosome profiling data (which revealed ICAM1 to be upregulated upon infection (FC = 1.62), but not of ICAM2 or VCAM1), we observed increased expression of ICAM1 (unpaired t-test with Welch's correction, *p*-value < 0.01), but not of ICAM2 (unpaired t-test with Welch's correction, *p*-value < 0.0001), nor VCAM1 (unpaired t-test with Welch's correction, *p*-value < 0.01) (Figure 4G). To determine whether the increase in ICAM1 was brain-specific, we checked ICAM1, ICAM2, and VCAM1 expression in remaining organs, and observed it also increased in the lungs, heart, and liver (unpaired t-test with Welch's correction, *p*-value < 0.01), whereas ICAM2 expression increased in the heart and kidneys (unpaired t-test with Welch's correction, *p*-value < 0.0001), and VCAM1 in the liver, spleen, and kidneys (unpaired t-test with Welch's correction, *p*-value < 0.01) (Figure S2A). Similar to what we did to assess the distribution of parasite load and sequestration, we asked whether the increase in ICAM1 expression was localized to a particular region in the brain. We observed that expression of ICAM1 increased in all anatomic regions of the brain, with the exception of the hypothalamus (Figure S2B and S2C).

In summary, analysis of the brain vasculature revealed that endothelial cells respond to *T. congolense* infection by displaying a pro-inflammatory response. IFNγ and/or associated cytokines (i.e. CXCL9, CXCL10), as well as genes involved in leukocyte transendothelial migration (i.e. ICAM1) may play a role in the development of *T. congolense* 1/148-associated neuropathology.

Blocking of ICAM1 reduces disease severity and parasite sequestration in the brain

The increase in ICAM1 expression in the brain endothelium, but not of ICAM2 or VCAM1 suggests that ICAM1 may play a role in disease severity, perhaps by favoring parasite sequestration and/or inflammation. We found previously that *T. brucei* interacts with several endothelial receptors (De Niz et al., 2021). To test if *T. congolense* sequestration depends on similar host molecules, we blocked ICAM1 *in vivo*, by administering α-ICAM1 antibody 24 hours before infection, repeating daily during the course of infection. We noticed that α-ICAM1-treated mice showed fewer signs of cerebral disease, so we used SHIRPA (i.e. SmithKline Beecham, Harwell, Imperial College, Royal London Hospital, phenotype assessment), a mouse phenotypic assessment protocol (Rogers et al., 1997), to test whether α-ICAM1-treated mice were neurologically fitter than isotype-treated controls.

We selected 5 parameters of the semi-quantitative SHIRPA protocol: posture, velocity of escape upon touching, positional passivity, type of locomotion, and grip strength. Mice infected with the strain 1/148 showed defects in all these parameters on day 6 post-infection (Figure 5A). These alterations are consistent with the changes described in dogs infected with *T. congolense* (Harrus et al., 1995), showing that SHIRPA protocol is a useful quantitative method to score neurological alterations associated to cerebral trypanosomiasis in this mouse model. The SHIRPA protocol revealed that α-ICAM1-treated mice performed better than the control group in all parameters relating to neurological impairment, and particularly those relating to movement and strength (Figure 5A). Importantly, we also found that α-ICAM1-treated mice survived longer than isotype-treated controls, as 50% of the mice were still alive at day 20 p.i, when the experiment was terminated (Figure 5B). Brain necropsy also showed reduced neuropathology (Figure 5C).

To understand the cellular basis of this ICAM1-dependent phenotype, we quantified parasite load and sequestration percentage in the brain at day 6 p.i., by intravital microscopy (Figure 5D). We found that total parasite load was unaffected by treatment (Figure 5E, left), but the percentage of cytoadhered parasites was reduced by 44% (2-way ANOVA, *p*-value = 0.0025) (Figure 5E, right). These results could suggest that ICAM1 directly promotes parasite sequestration. To test if ICAM1 is a potential receptor for parasite adhesion, we immobilized recombinant ICAM1, CD36 and BSA on a plastic surface, in static conditions, and measured 1/148 parasite adherence by microscopy after a 30-minute incubation (Figure 5F). Parasites did not adhere more to recombinant ICAM1 protein than to either BSA or recombinant CD36 protein (Figure 5G), suggesting that parasite sequestration is not mediated by ICAM1 binding.

These data show that blocking ICAM1 reduces parasite sequestration in the brain, improves disease severity and promotes survival, but this effect appears to be independent of direct parasite binding to the ICAM1 receptor.

T. congolense **1/148 infection results in an increase in the number of circulating ICAM1$^+$ monocytes**
Given that ICAM1 is important in leukocyte recruitment and infiltration (Lawson and Wolf, 2009), next we investigated whether the phenotypic effect of ICAM1 blocking could derive from an impaired immunological response. First, we measured the impact of ICAM1 blocking in the number of circulating nucleated cells specifically in the brain vasculature. By intravital imaging, we detected a 67%±5% reduction in the number of circulating nucleated cells (assumed to be leukocytes due to their size and complexity) (one-way ANOVA, *p*-value = 0.0270), which was not observed when blocking either ICAM2 or VCAM1 (Figure 6A and 6B). These results indicate that the ICAM1 blocking may improve disease outcome by reducing the magnitude of the immune response.

Next, we characterized the immune response in the systemic circulation at day 6 p.i. using flow cytometry. We observed no significant changes in the number of myeloid cells (i.e. dendritic cells, monocytes and macrophages) at day 6 post-infection (Figure 6C), but the number of B cells was 1.63-fold reduced (2-way ANOVA, *p*-value = 0.0277) (Figure 6D). Interestingly, ICAM1$^+$ monocytes in the blood increased 13-fold upon infection (2-way ANOVA, *p*-value < 0.0001) (Figure 6E).

Then, we characterized the leukocyte populations within the brain and within the brain vasculature. Thus, to distinguish and quantify the number of intra- and extravascular leukocytes, we administered α-CD45-APC antibody intravenously, 3 minutes prior to mouse euthanasia. In such a short incubation time, the antibody does not traverse the vasculature and thus only stains intravascular leukocytes (Anderson et al., 2014; Morawski et al., 2017). Figure S3A confirms that the α-CD45-APC antibody was efficient at staining intravascular leukocytes. As expected, we found an increase in the number of both extravascular (unpaired t-test, *p*-value = 0.0482, t = 2.813, df = 4) and intravascular (unpaired t-test, *p*-value = 0.0160, t = 4.0007, df = 4) $CD45^+$ cells upon infection (Figure S3B). Additionally, the contribution of intravascular leukocytes to the total immune cells in the brain is higher in infected animals (14% ± 4 *vs.* 25% ± 1).

Leukocytes are a heterogenous population of cells. To characterize the changes within the myeloid (e.g. monocytes, macrophages and dendritic cells) and lymphoid (B and T cells) subpopulations, we stained brain leukocytes for various subset markers, and quantified them using flow cytometry (Figure S4). We did not stain for neutrophils because preliminary experiments revealed that neutrophil numbers do not change significantly upon infection (Figure S3C). As expected, the numbers of extravascular DCs and monocytes was low in both infected and non-infected conditions. However, the number of $CD11b^+F4/80^+$macrophages increased 2.4-fold upon infection, suggesting infiltration of circulating inflammatory monocytes into the brain parenchyma (2-way ANOVA, *p*-value < 0.0001) (Figure 6F). In contrast, the number of intravascular $CD11b^+CD11c^+$ dendritic cells (DC) and $CD11b^+Ly6C^+$ monocytes increased by 8-fold (2-way ANOVA, *p*-value = 0.0113, < 0.0001, respectively) (Figure 6G). Importantly, 93 ± 16% of the intravascular monocytes expressed ICAM1 during infection (Figure 6H) and at higher mean fluorescent intensity (MFI) (2013 ± 206 in non-infected *vs.* 2962 ± 206 in infected mice, 2-way ANOVA, *p*-value = 0.0006) (Figure S3D), compared to only 32 ± 14% in the non-infected control, which is reflected in a significant increase (91-fold) in the number of ICAM1-expressing monocytes circulating in the brain vasculature (2-way ANOVA, *p*-value < 0.0001) (Figure 6H).

The numbers of lymphoid cells present in the brain showed a tendency to increase, but this effect was reflected in both extravascular and intravascular populations (Figure 6I and 6J). The numbers of extravascular B cells increased 5-fold, CD4+ T helper cells increased 9-fold, and CD8+ cytotoxic T cells increased 8-fold. Whilst the number of intravascular B cells remains similar upon infection, the number of CD4+ T helper cells and CD8+ cytotoxic T cells increased 4.5 and 4.7-fold, respectively. In terms of ICAM1 expression, barely any T cells were detected to express ICAM1 regardless of infection status, whereas the number of $ICAM1^+$ extravascular B cells increased 13-fold (2-way ANOVA, *p*-value < 0.0353) (Figure 6K).

These data show that, upon infection, the development of cerebral trypanosomiasis is associated with the recruitment of myeloid cells to the brain vasculature, most of which express ICAM1.

Cerebral animal African trypanosomiasis is prevented in the absence of T cells

To test if the increase in circulating monocytes cells is the cause of cerebral trypanosomiasis, we depleted circulating monocytes and inflammatory macrophages by intravenous administration of clodronate liposomes 24 hours prior and 3 days post-infection. We observed that mice treated with

clodronate liposomes showed high peripheral parasitaemia earlier than mice receiving either PBS-filled liposomes or PBS only (Figure S5A). Survival was also affected. Mice receiving clodronate liposomes, died between days 6 and 7, compared to days 7-8 when receiving control liposomes, and days 7-10 if only PBS was administered (Figure S5B). Moreover, we performed mouse behavioral assessment on day 6 post-infection and observed that monocyte/macrophage depletion increased severity of neurological impairment (Figure S5C). These results show that neuropathology cannot be specifically attributed to monocytes/inflammatory macrophages, as these cells seem to have a principal protective effect against infection.

In other parasitic diseases, like cerebral malaria, brain immunopathology is caused by small numbers of infiltrating $CD8^+$ T cells (Belnoue et al., 2002). Moreover, upregulation of ICAM1, IFNγ, and related cytokines is known to increase T cell adhesion and transendothelial cell migration (Ashok Sonar et al., 2017; May and Ager, 1992; Sancho et al., 1999). Thus, we hypothesized that T cells could cause neuropathology. We used mice of the same genetic background, but that do not produce mature T and B cells (RAG2 KO mice) to directly investigate the role of T cells in parasite sequestration and pathology in the brain. Although they also lack mature B cells, mice with cerebral trypanosomiasis do not survive past the first peak of parasitemia, so the antibody-mediated response is unlikely to play an important role in ICAM1-mediated neuropathology. Besides, we did not observe a significant variation in B cell numbers in the brain upon infection.

We performed intravital microscopy in the brain of RAG2 KO mice infected with *T. congolense* 1/148 at day 6 p.i. (Figure 7A) and quantified the number of circulating nucleated cells. We observed that it was reduced relative to WT mice and similar to the levels observed in α-ICAM1-treated mice (Figure 7B and Figure 6B). When we followed disease progression, we observed that RAG2 KO mice performed better than WT in every parameter of the SHIRPA test, with only one mouse (out of five) showing signs of neurological impairment (Figure 7C). As expected due to the absence of B cells, mice did not clear parasitaemia, and remained heavily parasitized, with minor oscillations (Figure 7D). Remarkably, unlike WT controls, mice survived up to day 40 p.i. (Figure 7E). Brain necropsy corroborated these observations as the level of brain lesions was lower overall, despite one mouse still showing moderate neuropathology (Figure 7F). These data suggest that neuropathology associated with cerebral trypanosomiasis is mainly due to T cells.

Given our previous results indicating a role of ICAM1 in cerebral trypanosomiasis, we investigated whether T cells could cause neuropathology via ICAM1 signaling. Therefore, we administered α-ICAM1 or its isotype control into RAG2 KO mice and infected them with *T. congolense* 1/148 parasites. At day 6 p.i., α-IgG2-treated RAG2 KO mice had similar parasite load in the vasculature of the brain to WT (Figure 7G), but presented lower levels of parasite sequestration (2-way ANOVA, *p*-value = 0.0241) (Figure 7H). This phenotype is similar to what we observed in α-ICAM1-treated WT mice (Figure 5E). Furthermore, we observed that α-ICAM1-treatment caused no effect on RAG2 KO mice in terms of both parasite load and percentage of parasite sequestration (Figure 7G and 7H), which shows that ICAM1 depletion plays no additional role when T cells are absent.

Discussion

Animal African trypanosomiasis comprises a spectrum of diseases. In this work, we established a mouse model of cerebral trypanosomiasis. We show that C57BL6/j mice infected with *T. congolense* 1/148 strain show significant and quantifiable neurological clinical signs, which are associated to parasite prolonged sequestration in the brain vasculature and an overwhelming ICAM1-mediated pro-inflammatory immune response.

Immunopathology in cerebral animal African trypanosomiasis

In the acute disease caused by strain 1/148, the brain is the site of preferential parasite sequestration. The presence of *T. congolense* has previously been shown to result in endothelium activation via the release of soluble factors *in vitro* (Ammar et al., 2013). Given our observations of *T. congolense* 1/148 parasites accumulating in the brain vasculature and having a prolonged interaction with the endothelium, we propose that parasite sequestration further enhances endothelial activation *in vivo*. Ultimately, tropism to the brain vasculature is a virulence factor and is a common feature of intravascular parasites. Trypanosome sequestration on the brain endothelium seems to cause the vascular occlusion that results in ischemia and tissue hypoxia, accounting for some of the pathological lesions we observed in infected mice. In both cerebral malaria and acute babesiosis, attenuation of strain virulence is accompanied by loss of cerebral capillary sequestration (Dondorp et al., 2004; Medana and Turner, 2006; Sondgeroth et al., 2013), much like what we observed when comparing *T. congolense* strains 1/148 and IL3000.

Ribosome profiling shows that brain endothelial cells respond to *T. congolense* infection strongly, by upregulating angiogenic and proinflammatory pathways. These responses include upregulation of genes involved in the increase of vascular permeability and vasodilation, as well as the recruitment and activation of innate and adaptive immune cells. Currently, we do not know whether the endothelium is activated by the direct effect of prolonged parasite sequestration, or due to the immune response. Upregulation of IFNγ, CXCL9, CXCL10, and ICAM1 suggests that neuroinflammation is caused by the activation of IFNγ−dependent and NF-κB pathways (Ashok Sonar et al., 2017; Lawson and Wolf, 2009; Luster et al., 1985; Medoff et al., 2005; Michlmayr and Mckimmie, 2014), which is corroborated by our current understanding of cerebral malaria pathogenesis (Favre et al., 1999; Tripathi et al., 2006; Yipp et al., 2000). Ultimately, the fact that RAG2 KO mice, but not monocyte/macrophage-depleted mice, survive four times more that WT suggests that T cells are the basis of cerebral trypanosomiasis.

T cell suppression by cyclosporine A administration has been shown not alter disease course nor associated inflammation in chronic models of trypanosomiasis (Noyes et al., 2009). In contrast, we would expect that the same treatment in a 1/148 infection would result in prolonged survival, mimicking the effect we observed in RAG2 KO mice. Moreover, although ICAM1 is upregulated in endothelial cells during IL3000 co-culture (Ammar et al., 2013), it does not result in life-threatening neuroinflammation (Figure 1C). This suggests that, whilst the exacerbated immune response may be the cause of neuropathology, parasite tropism to the brain, and the consequent increase in parasite sequestration, may

be essential for the development of cerebral trypanosomiasis. This mechanism may not be triggered in IL3000 infections because of the reduced parasite sequestration in the brain.

We propose a model for the mechanism of disease of cerebral trypanosomiasis (Figure 8). Upon adhesion to endothelial cells, the parasite releases pro-inflammatory soluble molecules, such as trans-sialidades, and causes activation of the endothelium via the NF-κB pathway (Ammar et al., 2013). This would result in the observed increase in ICAM1 expression in the plasma membrane of endothelial cells. Ultimately, parasite sequestration could trigger a pro-inflammatory response, possibly mediated by IFNγ-dependent and the NF-κB pathway. Pro-inflammatory cytokines lead to the increase in circulating myeloid cells in the brain, particularly of ICAM1^{+} monocytes. Some of the monocytes cross the BBB, accumulate in the brain and differentiate into macrophages. These cytokines, chemokines and myeloid cells also promote T cell recruitment to the brain vasculature (Clark et al., 2007). T cells interact with ICAM1 at the surface of endothelial cells, and possibly myeloid cells, which facilitates activated T cell adhesion and extravasation to the brain parenchyma (Dietrich, 2002). We propose this is the cause of the immunopathology that culminates in cerebral trypanosomiasis.

The similarities of the *T. congolense*-associated neuropathology with that of cerebral malaria are clearly remarkable, but perhaps not unexpected if we reconsider that the initial events that trigger the immune response, namely sequestration and endothelial damage, are alike. ICAM1 is one the endothelial cell adhesion receptors for *P. falciparum* (Berendt et al., 1989), but has a multifaceted role in cerebral malaria pathogenesis (Storm and Craig, 2014). Whilst we did not find evidence for ICAM1 to be an endothelial cell receptor for *T. congolense* parasites, this hypothesis cannot be excluded until more sensitive and complex adhesion assays are performed. Both IFNγ and CXCL10 play important roles in the inflammation that drives cerebral malaria-associated neuropathology, namely in terms of T cell adhesion to endothelial cells (Sorensen et al., 2018), and recruitment to the brain parenchyma (Campanella et al., 2008). Monocytes promote brain inflammation, secretion of IFNγ, and activation of CD8^{+} T effector cells (Schumak et al., 2015).

Advantages of parasite sequestration

Our data shows that *T. congolense* parasites of both 1/148 and IL3000 strains sequester in the vasculature of major organs, albeit to different degrees. Previous studies of *T. congolense* in experimental and natural infections are consistent with our observations (Fiennes, 1952; Losos and Gwamaka, 1973; Losos et al., 1971; Maxie and Losos, 1977). It emerges that sequestration is a trait of *T. congolense* as a species and an essential mechanism of interaction with the mammalian host. However, sequestration is not a characteristic of all African trypanosomes. *T. brucei* parasites, for instance, do not sequester (Silva Pereira et al., 2019). Although they interact with the endothelium and may in fact adhere to it, *T. brucei* parasites do it as means to invade the extravascular spaces of tissues (De Niz et al., 2021). So, why is it more advantageous for *T. congolense* to sequester, but for *T. brucei* to cross the endothelium? Other parasites employing sequestration, like *P. falciparum* and *B. bovis*, do so to evade the immune response and prevent splenic clearance of infected red blood cells (Allred and Al-Khedery, 2004; Dinko and Pradel, 2016). However, being extracellular, trypanosome clearance is not exclusively spleen-dependent. Some

IL3000 parasites remain cytoadhered after the antibody-mediated clearance that follows the peaks of parasitemia, suggesting sequestration may help to keep enough parasites to start a new wave of parasitaemia. Nonetheless, clearance of *T. brucei* from the blood is also not entirely efficient (De Niz et al., 2021), which indicates that sequestration is not a requirement for parasite persistence, even in the absence of tissue invasion.

Morphological and physiological characteristics of *T. congolense* parasites facilitate sequestration: they can cytoadhere with any part of the cell and have a rounder cell shape, stiffer cell body, and shorter flagellum that results in slower motility (Bargul et al., 2016). Cytoadhesion requires considerable force to counteract the speed of the blood blow, so these features may help reduce energy expenditure. Simultaneously, it is possible that sequestration enhances parasite-endothelium interactions by facilitating hijacking of cellular functions and/or host's nutrients. For instance, sequestration might facilitate iron uptake, which is both essential for trypanosome survival and a source of host pathology due to anemia (Stijlemans et al., 2015). It would be interesting to test whether cytoadhered *T. congolense* parasites are functionally different from circulating parasites and for example, express higher levels of transferrin or haptoglobin-hemoglobin receptors, necessary for iron and hem internalization, respectively. Our work lays the ground for more detailed examinations of sequestration, including the characterization of movement type, binding forces and receptor-ligand interactions.

In conclusion, we show that cerebral trypanosomiasis is caused by the combination of parasite sequestration in the brain and immune cell recruitment, and consequently can be prevented. As we reveal that *T. congolense* sequestration is a virulence factor, we bring a novel hypothesis forward: trypanosome sequestration patterns can determine strain virulence, and thus the risk of disease severity. The translation potential of our findings is large as they expose possible drug treatment strategies targeting mediators of sequestration and/or immunomodulators, as well as to the design of targeted strategies for vector control and surveillance frequency, when coupled with epidemiological mapping.

Declarations

Acknowledgments

We thank Dr Álvaro Acosta-Serrano, at the Liverpool School of Tropical Medicine, and Dr Loïc Rivière for providing *T. congolense* 1/148 and IL3000 parasite lines, respectively. We also thank Dr Joana Coelho for helpful training on the SHIRPA protocol. We thank the Silva-Santos lab for the providing the RAG2 KO mice. We are grateful to Dr Margarida Vigário and Dr Joana Coelho for careful reading of the manuscript. We thank the Rodent and Bioimaging facilities and the Comparative Pathology Unit (including previous members Pedro Ruivo, DMV and Dr Tânia Carvalho, DMV) at iMM. This work was supported by European Union's Horizon 2020 research and innovation program through a Marie Skłodowska-Curie Individual Standard European Fellowship to S.S.P., under grant agreement no. 839960, and from the European Research Council (ERC) (FatTryp, ref. 771714) to L.M.F.. M.D.N. was funded by Human Frontiers LT000047/2019-L (HFSP) and EMBO (ALTF 1048-2016). L.M.F., K.S., and C.A.F. are Investigators

CEEC of the Fundação para a Ciência e a Tecnologia (CEECIND/03322/2018, CEECIND/00697/2018, CEECIND/04251/2017, respectively). C.A.F. was supported by a European Research Council starting grant (679368), the Fondation Leducq (17CVD03), and the Fundação para a Ciência e a Tecnologia (grants IF/00412/2012, EXPL/BEX- BCM/2258/2013, PRECISE-LISBOA-01-0145-FEDER-016394, PTDC/MED-PAT/31639/2017, PTDC/BIA-CEL/32180/2017).

Author Contributions

Conceptualization, S.S.P., M.D.N., K.S., C.A.F., and L.M.F.; Methodology, S.S.P., M.D.N., and L.M.F.; Investigation, S.S.P., M.D.N., M.O.; Writing – Original Draft, S.S.P., M.D.N., and L.M.F.; Funding Acquisition, S.S.P., M.D.N., and L.M.F.; Resources, K.S., C.A.F., and L.M.F.; Supervision, L.M.F.

Declaration of Interests

The authors declare no competing interests.

Star Methods

Animal Experiments

This study was conducted in accordance with EU regulations and ethical approval was obtained from the Animal Ethics Committee of Instituto de Medicina Molecular (AWB_2016_07_LF_Tropism). Infections were performed at the rodent facility of Instituto de Medicina Molecular, in 6–10 weeks old, wild-type, male C57BL/6J mice (Charles River, France), RiboTag.PDGFb-iCRE mice, or RAG2 KO mice of the same age, bred in-house. Mice were infected by intraperitoneal injection (i. p.) of 2 x 10^3 [*T. congolense* savannah 1/148 (MBOI/NG/60/1-148) (Young and Godfrey, 1983)] or 2 x 10^4 [*T. congolense* savannah IL3000 (Gibson, 2012)] parasites, under mild isoflurane anesthesia. Parasitemia was estimated daily by hemocytometry from tail venipuncture. Mice were sacrificed by anesthetic overdose (intravital and ex-vivo microscopy), cervical dislocation (flow cytometry) or CO_2 narcosis (all remaining experiments). Blood was collected by heart puncture and, when necessary, mice were perfused with 50 ml heparinized PBS. Tissues were dissected, washed in PBS and immediately imaged, snap frozen in liquid nitrogen, or fixed in 10% neutral-buffered formalin.

Histology and Immuno-histochemistry

Formalin-fixed organs were embedded in paraffin and 3 µm sections were stained with hematoxylin and eosin (H&E). For immunohistochemistry, 3 µm sections were immunostained with a non-purified rabbit serum α-*T. brucei* histone 2A (H2A) (generated against a recombinant protein) (kind gift of Christian Janzen), diluted 1:5000. Antigen heat-retrieval was performed in a microwave oven (800 W) for 15 minutes with pH 9 Sodium Citrate buffer (Leica Biosystems, MO, USA). Incubation with ENVISION kit (Peroxidase/DAB detection system, Dako Corp, Santa Barbara, CA) was followed by Mayer's hemalumen

counterstaining. Tissue sections were examined by a pathologist, blinded to experimental groups, in a Leica DM2500 microscope coupled to a Leica MC170 HD microscope camera.

Surgical Procedures and Intravital Microscopy

For intravital microscopy, surgeries were separately performed by groups of organs, as previously described for the brain (De Niz et al., 2019a), the lungs and heart, the liver, pancreas, spleen and kidneys (De Niz et al., 2020), and the adipose tissues (De Niz et al., 2019b). In summary, mice were anaesthetized prior to surgery with a mixture of ketamine (120 mg/kg) and xylazine (16 mg/kg), by intraperitoneal injection. Reflex responses were induced, and surgery was initiated once these responses were non-existent. For all experiments used for quantification of cytoadhered and flowing parasites, mice were injected with 3 markers: Hoechst 33342 to label nucleic acids, 70 kDa FITC-Dextran to label the intravascular space and provide contrast within the vessel walls, and a fluorescently conjugated antibody against the pan-vascular marker CD31 (PECAM1). Prior to surgery, mice were intraocularly injected with Hoechst 33342 (stock diluted in dH2O at 100 mg/ml, injection of 40 µg/kg mouse), 70 kDa FITC-Dextran (stock diluted in 1x PBS at a concentration of 100 mg/ml, injection of 500 mg/kg mouse), and A637-CD31 (BioLegend, used at 20 µg/mouse). For imaging, a temporary glass window (Merk rectangular cover glass, 100 mm x 60 mm) or a circular cover glass (12 mm) was implanted in each organ. The windows were secured surgically using stitches, or immobilized using surgical glue. For imaging the heart and lungs, the windows were immobilized using a vacuum to prevent collapse of the thoracic cavity.

All intravital microscopy performed with the aim of identifying flowing and circulating parasites was performed in spinning disc microscopes. These included a Zeiss Cell Observer SD (Carl Zeiss Microimaging, equipped with a Yokogawa CSU-X1 confocal scanner, and an Evolve 512 EMCCD camera and a Hamamatsu ORCA-Flash 4.0 VS camera) or a 3i Marianas SDC (spinning disc confocal) microscope (Intelligent Imaging Innovations, equipped with a Yokogawa CSU-X1 confocal scanner and a Photometrics Evolve 512 EMCCD camera). Laser units 405, 488, and 647 were used to image Hoechst, FITC-Dextran and AF67-CD31 respectively. Visualization was done using either an oil-immersion plan apochromat 63x objective with 1.4 NA and 0.17 WD, or a 40x LD C-Apochromat corrected, water immersion objective with 1.1 NA and 0.62 WD. Images were obtained for a total of 20 seconds, at an acquisition rate of 20 frames per second. For all acquisitions, the software used was either ZEN blue edition v.2.6., or 3i Slidebook reader v.6.0.22.

For the quantification of the duration of sequestration in the brain, longer imaging sessions were required. Therefore, *T. congolense*-infected mice were imaged at day 6 post-infection for a total of 12 hours, with images acquired every 30 minutes. In this case, a non-invasive cranial window was implanted on the skull, and anesthesia was injected every hour intraperitoneally, in addition to inhalable anesthesia (isoflurane) being supplied as required to ensure analgesic and anesthetic effect for the full imaging time. Cytoadhered parasites were defined as those that did not change positions relative to the immediately preceding time, in half-hourly periods.

Ex-vivo Microscopy

While intravital imaging in living mice mostly allows visualization of parasite-host interactions in the cerebral cortex, the meninges, and the olfactory bulb, we were interested in visualizing parasite dynamics throughout the entire brain. For this purpose, we followed the same procedures as previously described for vascular and nucleic acid labeling, and we then surgically exposed ten different regions of the mouse brain, namely the olfactory bulb, the cerebral cortex, the septum, the hypothalamus, the thalamus, the hippocampus, the midbrain, the pons, the medulla, and the cerebellum. Imaging was performed within a humid chamber with 37°C stable temperature and oxygen flow to delay loss of oxygenation and therefore alter parasite dynamics. Using these conditions parasites retain their motility for an average of 1 hour, during which we quantified cytoadhered and flowing parasites in the vascular area of each region.

Image Analysis

Quantification of cytoadhered and flowing parasites

In order to quantify cytoadhered and flowing parasites, we used as reference the 70 kDa FITC-Dextran and the Hoechst 33342. On one hand, the FITC-Dextran enabled identification of the parasite bodies by the contrast generated in the vascular space. Meanwhile, the Hoechst 33342 which stains nucleic acids, allowed clear labeling of the nucleus and kinetoplast of *T. congolense* parasites. Flowing parasites were defined as those displacing along the field of view throughout the time-lapse acquisition, together with the red blood cells (also identifiable by the contrast achieved by the FITC-Dextran within the vessel wall). Cytoadhered parasites were defined as those not displaying throughout the time-lapse acquisition. These parasites often displayed movement of the body and flagellum, but despite these local movement, the bodies remained attached at the same spot of the vessel wall. To enable quantifications by vascular area, we determined the total area of the field of view, and extracted the vascular area using the FITC-Dextran and AF647-CD31. We calculated the percentage of vascular area (Av%) using the formula $A_{v\%} = \frac{A_v \times A_{T\%}}{A_T}$, where A_T is the total area of the field of view, A_T is 100% and A_v is the total area marked by FITC-Dextran and CD31. Then, we normalized the total quantity of cytoadhered and flowing parasites, to the calculated vascular area. These measurements were performed daily in *T. congolense* Tc1/148-infected C57BL/6J mice, throughout 6 days of infection, at peaks of infection in *T. congolense* IL3000-infected C57BL/6J mice, and at day 6 of infection in several antibody-treated C57BL/6J mice as well as RAG2 KO mice. In addition to vascular area, we quantified vascular diameter of vessels in each field of view, to calculate number of adhered and cytoadhered parasites in 4 categories of vessel diameters (0-10 µm, 10-20 µm, 20-40 µm, and > 40 µm). Vascular area and diameter measurements were calculated using Fiji software.

Quantification of parasite region enabling sequestration

To evaluate and quantify parasite regions enabling sequestration, we used spinning disc confocal microscopy as previously described. Visualization was done using an oil-immersion plan apochromat 100X objective with 1.4 NA and 0.17 WD. Throughout 5 minutes of time-lapse imaging at a rate of 20 frames per second, we determined whether cytoadhered parasites remained attached using the mid-body, the parasite posterior, the flagellar tip, or variable. The latter was defined as several regions of the parasite involved in sequestration, with the attachment point shifting throughout the time lapse imaged.

Quantification of kinetoplast and nuclear numbers, and nuclear area

To quantify nuclear and kinetoplast numbers, and nuclear area in cytoadhered and flowing parasites, visualization was done using an oil-immersion plan apochromat 100x objective with 1.4 NA and 0.17 WD. In order to visualize the full parasite body, we generated confocal images of 12-16 stacks, with step sizes of 0.2 mm. To be able to capture the entire parasite body, we surgically stopped blood flow. This resulted in flowing parasites continuing to displace, while cytoadhered parasites remained in the same position throughout the entire time-lapse acquired. Using the contrast generated by the FITC-Dextran, we defined the parasite regions, and classified parasites into 3 categories: those having 1 kinteoplast and 1 nucleus (1K1N), 2 kinetoplasts and 1 nucleus (2K1N), and 2 kinetoplasts and 2 nuclei (2K2N). Of important note, the distance between the two nuclei in both *T. congolense* strains used in this work, is much smaller than the one observed in *T. brucei* parasites. For this reason, we also measured nuclear area. Nuclear segmentation was facilitated by the use of Hoechst 33342, and measurements were performed using Fiji software.

Leukocyte quantification by intravital microscopy

Intravital microscopy allowed us to observe an increase of nucleated, large cells in the vasculature of the brain in infected mice. This visualization is achieved by the contrast provided by the 70 kDa FITC-Dextran, and the nuclear labeling allowed by Hoechst 33342. Although these combined dyes do not allow the definition of types and sub-types of leukocytes during infection, they allow segmentation and quantification of new cell populations compared to control uninfected mice. Having obtained information from intravital microscopy, we characterized immune cell populations in infected animals by flow cytometry, using specific antibodies as described below.

Endothelial cell polysome immunoprecipitation and RNA sequencing

Cre recombinase activity was induced in RiboTag.PDGFb-iCRE mice by daily i. p. injection of 10uL/g mouse weight of 8mg/mL of tamoxifen (Sigma Aldrich, T5648), diluted in 10% ethanol and 90% peanut oil (Sigma Aldrich, P2144), for five days. Mice were left to recover for 72 hours before infection with $2x10^3$ *T. congolense* 1/148 parasites. Age and sex-matched mice were used as non-infected controls. Mice were euthanized at days 6 post-infection and perfused with 50ml heparinized PBS. Brains were dissected, cut in half and homogenized in supplemented homogenization buffer (50 mM Tris, pH 7.5, 100 mM KCl, 12 mM $MgCl_2$, 1% Nonidet P-40, 1 mM DTT, 200U/mL Promega RNasin, 1 mg/mL heparin, 100 µg/mL cycloheximide, Sigma protease inhibitor mixture) using a 2ml dounce homogenizer and glass pestles.

Ribosomes of the endothelial cells were immunoprecipitated according to Sanz et al. (2009). Briefly, homogenized brains were incubated with 4µl of α-HA.11 Epitope Tag Antibody (BioLegend, UK) for 2 hours at 4ºC; polysomes bound to α-hemagglutinin antibody were immunoprecipitated using Pierce A/G magnetic beads (ThermoFisher Scientific, Spain) previously washed in homogenization buffer (50 mM Tris, pH 7.5, 100 mM KCl, 12 mM MgCl2, 1% Nonidet P-40). Beads bound to antibody-polysome conjugation were washed with high salt buffer (50 mM Tris, pH 7.5, 300 mM KCl, 12 mM $MgCl_2$, 1% Nonidet P-40, 1 mM DTT, 100 µg/mL cycloheximide) and dissociated by chemical and mechanical lysis. RNA was extracted using the RNeasy Mini kit (Qiagen, UK).

RNA concentration and integrity were checked by fluorometry (Qubit DNA HS, Thermo Fisher Scientific) and parallel capillary electrophoresis (Fragment Analyzer, BioLabTech), respectively. cDNA libraries were prepared using the QuantSeq 3' mRNA-Seq Library Prep Kit FWD for Illumina (Lexogen, Austria), as per manufacturer instructions, and sequenced as 75bp single-end reads on the NextSeq 550 platform (Illumina, USA). Reads were aligned to the mouse genome GRCm39 (http://www.ensembl.org/Mus_musculus/Info/Index) using STAR (Dobin et al., 2013). The output from read alignment was processed with SAMtools (Li et al., 2009), and transcript abundances were estimated using stringtie (Pertea et al., 2015). Differential expression between input and immunoprecipitated samples was performed in R, using the EdgeR (McCarthy et al., 2012; Robinson et al., 2010) and limma-voom (Law et al., 2014) packages, as previously published (Smyth et al., 2018). Log2 Fold change of 1 and p-value < 0.05 was considered significant. Gene Set Enrichment Analysis (GSEA) (Subramanian et al., 2005) was performed using the WEB-based GEne SeT AnaLysis Toolkit (WebGestalt) (Wang et al., 2017). Non-expressed genes were removed from the analysis and the remaining were ranked by differential expression Log2 fold change. Gene sets were defined based on gene ontology for biological function.

Cytokine Profiling

Blood was collected from mice either non-infected or infected with *T. congolense* 1/148 at days 3 and 6 post-infection by cardiac puncture. Blood was allowed to clot for 30 minutes at room temperature and then centrifuged at 1000 x g for 10 minutes at 4ºC. Serum was collected from each sample and added to an equal volume of PBS (pH 7.4). Samples were immediately frozen at -80ºC, and shipped in dry ice to Eve Technologies (Canada), where a Mouse Cytokine Array / Chemokine Array 31-Plex was performed, in duplicate.

Receptor Expression by Mean Fluorescent Intensity

To investigate the relative expression of endothelial receptors in different organs, we intravenously injected 20 µg per mouse, of fluorescently conjugated antibodies against ICAM1, ICAM2 (BioLegend, conjugated to AF647), and VCAM1 (Invitrogen, conjugated to FITC). These were administered intravenously, by retroorbital injection, into either non-infected mice or mice infected with *T. congolense* 1/148 at day 6 of infection. We measured mean fluorescent intensities of at least 100 vessels per organ in 3 separate mice using an LSM 880 Zeiss microscope, and a 40x oil objective (1.3 NA).

Blocking Antibody Binding Assay

Mice were treated daily with 2 µg of α-ICAM1 antibody [CD54 monoclonal antibody (YN1/1.7.4), #16-0541-85, Invitrogen], or rat α-IgG2b kappa isotype control (eB149/10H5), #16-4031-81, Invitrogen), diluted in 200µl PBS via retro-orbital intravenous injection, under isoflurane anesthesia. Twenty-four hours after the first antibody treatment, mice were infected with *T. congolense* 1/148 parasites as described above.

rICAM1 Static Adhesion Assay

To test the capacity of *T. congolense* 1/148 parasites to bind to ICAM1 in vitro, we performed a static adhesion assay. Plastic cell culture-grade 48-well plates (Corning, USA) were coated with 100 µl of protein A (#6500B, BioVision) diluted at 20µg/ml in PBS (pH 9.0) and incubated in a cell culture incubator for 1 hour at 37ºC, 5% CO2. Plates were washed three times with PBS (pH 7.4) to remove unbound protein, blocked with 200µl of 1% bovine serum albumin (BSA), and incubated at 4ºC overnight. Subsequently, plates were washed with PBS (pH 7.4) to remove unbound BSA,100 µl of purified recombinant mouse FC chimera protein [rICAM1 or rCD36 (#796-IC-050 and # 2519-CD-050, R&D Systems)], diluted at 25 µg/ml were spotted in a radial pattern onto the center of the wells, and incubated in a cell culture incubator for 3 hours at 37ºC, 5% CO2. Plates were washed three times with PBS (pH 7.4) and 100 µl of BSA were added. Plates were incubated again for 30 minutes at 37ºC, 5% CO_2. Simultaneously, parasites were isolated from mouse by anion exchange chromatography (Lanham and Godfrey, 1970) and stained with 5mM Vybrant™ CFDA SE Cell Tracer dye (#V12883, Invitrogen) diluted 1000 times in trypanosome dilution buffer (TDB) (5 mM KCl, 80 mM NaCl, 1 mM MgSO4, 20 mM Na2HPO4, 2 mM NaH2PO4, 20 mM glucose, pH 7.4), and incubated for 25 minutes at 34ºC, 5% CO_2. At the end of the incubation period, parasites were washed and resuspended in TDB, added to the previously-washed pre-coated plates, and incubated for 1 hour at 34ºC, 5% CO_2. Plates were washed twice with PBS (pH 7.4) to remove unbound parasites. We added 100 µl of TDB to the washed plates, now containing only adhered parasites, and proceeded with live imaging on a Zeiss Cell Observer (Carl Zeiss Microimaging) with a 40X water-immersion objective. We acquired 15 fields of view per replicate well (3 replicates), per condition (BSA alone, rICAM1, rCD36) using bright-field light and green laser. We used Fiji software to count adhered parasite per field of view and total area imaged.

SHIRPA Test

We performed the primary screen of the previously described SHIRPA protocol (Rogers et al., 1997), consisting on the behavioral observation profiling of mice. The SHIRPA test allows assessment of muscle and lower motor neuron function, spinocerebellar function, sensory function, neuropsychiatric function, and autonomic function. The parameters assessed and their respective scores were: Locomotion: 0 – Completely flattened, 1 – Lying on the side, 2 – Lying upright, 3 – Sitting up, 4 – Standing on hindlimbs (Rearing) (Normal), 5 – Repeated vertical leaping; Posture: 0 – Normal, 1 – Hunched, 2 – No posture; Exploration/Spontaneous activity: 0 – Inactive, Resting, 1 – Active (Normal), 2 – Excessively Active; Movement Type (and tail posture): 0 – Normal movement, tail up, 1 – Walking well, but tail lagging

behind, 2 – Dragging the lower body, 3 – Inactive; Breath Rate: N(0)– Normal, L(1) – Labored, S(2) – Shallow, R(3) – Retching, D(4) – Dyspneic, G(5) – Gasping; Palpebral closure: 0 – Closed, 1 – Semi-opened, 2 – Opened/Normal 3 – Extremely opened; Touch Escape: 0 – None, 1 – Slow escape, 2 – Moderate/rapid escape (Normal), 3 – Rapid escape; Coat Appearance: N(0) – Normal grooming, normal density, P(1) – Moderate piloerection, PP(2) – Extreme piloerection; Positional Passivity: 0 – No struggle, 1 – Struggle, open limbs, 2 – Struggle, grasping limbs, closed paws, 3 – struggle, trunk curl; Grip Strength: Time (in seconds) that mice can hold upside down on a grid (Grid Test, maximum of 1 minute). All tests were performed in a new, clean cage, so that the mice would not be disturbed by cage mates.

Immune Cell Isolation, Staining and Flow Cytometry

Infected and non-infected mice were anaesthetized with isoflurane and received 3µg of α-APC-CD45 intravenously, by retroorbital injection. Antibodies were allowed to circulate for a maximum of three minutes, mice were euthanized by cervical dislocation, 50-150 µl of blood were collected by cardiac puncture, added to 2 ml ACK lysis buffer (155mM Ammonium Chloride, 10 mM Potassium Bicarbonate, 0.1 mM EDTA), left to incubate at room temperature for 15 minutes for red blood cell lysis, and centrifuged for 5 minutes at 550 x g, 4ºC. The supernatant was discarded the procedure repeated. At the end, the cell pellet was gently resuspended in RPMI 1640 medium (#11875093, Gibco) supplemented with 10% FBS (#10270106, Gibco). Brains were dissected, added to 5ml supplemented RPMI 1640 medium, cut in small pieces, and incubated with 100 µg/ml DNAse and 1.5 mg/ml collagenase D for 30 minutes at 37ºC with periodic agitation. After the incubation, an additional 15ml of medium were added, the organs were forced to pass through a 70 µm cell strainer, and centrifuged at 550 x g for 5 minutes at 4ºC. Resulting pellet was resuspended in 3 ml of 40% percoll and passed to a 15 ml tube, after which 2 ml of 70% percoll were slowly added to the bottom. Samples were centrifuged for 30 minutes at 2400 rpm with no acceleration or brake. The interphase was carefully collected with a pipette, added to 5ml of supplemented RPMI 1640 medium, and centrifuged at 550 x g for 5 minutes at 4ºC. The supernatant was discarded by inversion and the pellet resuspended in 2ml of supplemented RPMI 1640 medium. Isolated blood and brain immune cells were counted on a hemocytometer, and between 2.5 x 10^5 and 2 x 10^6 cells per sample stained with the following conjugated mouse antibodies: FITC-Ly6C (#128005, Biolegend), PE/CD11c (#117307, Biolegend), PerCP-Cy5.5-CD8 (#100733, Biolegend), PE/Cy7-F4/80 (#123113, Biolegend), PE/Dazzle-CD45 (#103145, Biolegend), Alexa Fluor 700-CD11b (#101222, Biolegend), APC/Cy7-CD4 (#100413, Biolegend), BV421-ICAM1 (#565987, BD Biosciences), BV605-CD19 (#563148, BD Biosciences), BV711-CD3 (#740739, BD Biosciences), BV785-MHCII (#107645, BD Biosciences), and CD16/CD32 FcR-blocking reagent (#553141, BD Biosciences). Live and dead cells were separated using BV510-Zombie Aqua™ fixable viability dye (4231010, Biolegend). Acquisition of mean fluorescence intensities was performed on the BD LSRFortessa™ X-20 Cell Analyzer equipped with a Violet (406 nm, 100 mW), Blue (adjustable 488 nm, 80 mW; maximum output 100 mW), Green (532 nm, 150 mW) and Red (642 nm, 40 mW) lasers, then analyzed with FlowJo v10 (TreeStar Technologies).

Monocyte/Macrophage Depletion

Circulating monocytes and inflammatory macrophages were depleted by intravenous retro-orbital injection of 1mg clodronate liposomes (Liposoma BV, The Netherlands) 24 hours prior to infection. Two control groups were included, one receiving PBS liposomes, and the other receiving PBS only. Treatment was repeated 3 days post-infection to maintain depletion.

References

Allred, D.R., and Al-Khedery, B. (2004). Antigenic variation and cytoadhesion in *Babesia bovis* and *Plasmodium falciparum*: Different logics achieve the same goal. Mol. Biochem. Parasitol. *134*, 27–35.

Ammar, Z., Plazolles, N., Baltz, T., and Coustou, V. (2013). Identification of Trans-Sialidases as a Common Mediator of Endothelial Cell Activation by African Trypanosomes. PLoS Pathog. *9*, e1003710.

Anderson, K.G., Mayer-Barber, K., Sung, H., Beura, L., James, B.R., Taylor, J.J., Qunaj, L., Griffith, T.S., Vezys, V., Barber, D.L., et al. (2014). Intravascular staining for discrimination of vascular and tissue leukocytes. Nat. Protoc. *9*, 209–222.

Ashok Sonar, S., Shaikh, S., Joshi, N., Atre, A.N., and Lal, G. (2017). IFN-γ promotes transendothelial migration of CD4+ T cells across the blood–brain barrier. Immunol. Cell Biol. *95*, 843–853.

Banks, K.L. (1978). Binding of *Trypanosoma congolense* to the walls of small blood vessels. J. Protozool. *25*, 241–245.

Banks, K.L. (1980). Injury Induced by *Trypanosoma congolense* Adhesion to Cell Membrane. J. Parasitol. *66*, 34–37.

Bargul, J.L., Jung, J., McOdimba, F.A., Omogo, C.O., Adung'a, V.O., Krüger, T., Masiga, D.K., and Engstler, M. (2016). Species-Specific Adaptations of Trypanosome Morphology and Motility to the Mammalian Host. PLOS Pathog. *12*, e1005448.

Belnoue, E., Kayibanda, M., Vigario, A.M., Deschemin, J.-C., Rooijen, N. van, Viguier, M., Snounou, G., and Rénia, L. (2002). On the Pathogenic Role of Brain-Sequestered αβ CD8 + T Cells in Experimental Cerebral Malaria . J. Immunol. *169*, 6369–6375.

Berendt, A.R., Simmons, D.L., Tansey, J., Newbold, C.I., and Marsh, K. (1989). Intercellular adhesion molecule-1 is an endothelial cell adhesion receptor for Plasmodium falciparum. Nature *341*, 57–59.

Berthier, D., Peylhard, M., Dayo, G.-K., Flori, L., Sylla, S., Bolly, S., Sakande, H., Chantal, I., and Thevenon, S. (2015). A Comparison of Phenotypic Traits Related to Trypanotolerance in Five West African Cattle Breeds Highlights the Value of Shorthorn Taurine Breeds. PLoS One *10*, e0126498.

van den Bossche, P., Chitanga, S., Masumu, J., Marcotty, T., and Delespaux, V. (2011). Virulence in *Trypanosoma congolense* Savannah subgroup . A comparison between strains and transmission cycles. Parasite Immunol. *33*, 456–460.

Campanella, G.S. V, Tager, A.M., Khoury, J.K. El, Thomas, S.Y., Abrazinski, T.A., Manice, L.A., Colvin, R.A., and Luster, A.D. (2008). Chemokine receptor CXCR3 and its ligands CXCL9 and CXCL10 are required for the development of murine cerebral malaria. Proc. Natl. Acad. Sci. *105*, 4814–4819.

Clark, P.R., Manes, T.D., Pober, J.S., and Kluger, M.S. (2007). Increased ICAM-1 Expression Causes Endothelial Cell Leakiness, Cytoskeletal Reorganization and Junctional Alterations. J. Invest. Dermatol. *127*, 762–774.

Dietrich, J.B. (2002). The adhesion molecule ICAM-1 and its regulation in relation with the blood-brain barrier. J. Neuroimmunol. *128*, 58–68.

Dinko, B., and Pradel, G. (2016). Immune Evasion by *Plasmodium falciparum* Parasites: Converting a Host Protection Mechanism for the Parasite's Benefit. Adv. Infect. Dis. *6*, 82–95.

Dobin, A., Davis, C.A., Schlesinger, F., Drenkow, J., Zaleski, C., Jha, S., Batut, P., Chaisson, M., and Gingeras, T.R. (2013). STAR: Ultrafast universal RNA-seq aligner. Bioinformatics *29*, 15–21.

Dondorp, A.M., Pongponratn, E., and White, N.J. (2004). Reduced microcirculatory flow in severe falciparum malaria: pathophysiology and electron-microscopic pathology. Acta Trop. *89*, 309–317.

Favre, N., Da Laperousaz, C., Ryffel, B., Weiss, N.A., Imhof, B.A., Rudin, W., Lucas, R., and Piguet, P.F. (1999). Role of ICAM-1 (CD54) in the development of murine cerebral malaria. Microbes Infect. *1*, 961–968.

Fiennes, R.N.T.-W. (1952). A Cryptic Focus of Parasites in Association With a Secondary Stage of Disease. Br. Vet. J. *108*, 298–306.

Ghazanfari, N., Mueller, S.N., and Heath, W.R. (2018). Cerebral Malaria in Mouse and Man. Front. Immunol. *9*, 2016.

Gibson, W. (2012). The origins of the trypanosome genome strains *Trypanosoma brucei brucei* TREU 927, T. b. gambiense DAL 972, T. vivax Y486 and T. congolense IL3000. Parasit. Vectors *5*, 71.

Harrus, S., Harmelin, A., Presenty, B., and Bark, H. (1995). *Trypanosoma congolense* Infection in two dogs. J. Small Anim. Pract. *36*, 83–86.

Hemphill, A., Frame, I., and Ross, C.A. (1994). The interaction of *Trypanosoma congolense* with endothelial cells. Parasitology *109*, 631–641.

Lanham, S.M., and Godfrey, D.G. (1970). Isolation of salivarian trypanosomes from man and other mammals using DEAE-cellulose. Exp. Parasitol. *28*, 521–534.

Law, C.W., Chen, Y., Shi, W., and Smyth, G.K. (2014). Voom: Precision weights unlock linear model analysis tools for RNA-seq read counts. Genome Biol.

Lawson, C., and Wolf, S. (2009). ICAM-1 signaling in endothelial cells. Pharmacol. Reports *61*, 22–32.

Li, H., Handsaker, B., Wysoker, A., Fennell, T., Ruan, J., Homer, N., Marth, G., Abecasis, G., and Durbin, R. (2009). The Sequence Alignment/Map format and SAMtools. Bioinformatics *25*, 2078–2079.

Losos, G.J., and Gwamaka, G. (1973). Histological examination of wild animals naturally infected with pathogenic African trypanosomes. Acta Trop. *30*, 57–63.

Losos, G.J., and Ikede, B.O. (1972). Review of Pathology of Diseases in Domestic and Laboratory Animals Caused by *Trypanosoma congolense*, *T. vivax*, *T. brucei*, *T. rhodesiense* and *T.gambiense*. Vet. Pathol. *9*.

Losos, G.J., Paris, J., Wilson, A.J., and Dar, F.K. (1971). Distribution of *Trypanosoma congolense* in tissues of cattle. In Thirteen Seminar on Trypanosomiasis, p. 287.

Luster, A.D., Unkeless, J.C., and Ravetch, J. V. (1985). γ-Interferon transcriptionally regulates an early-response gene containing homology to platelet proteins. Nat. 1985 3156021 *315*, 672–676.

Mamoudou, A., Njanloga, A., Hayatou, A., Suh, P.F., and Achukwi, M.D. (2016). Animal trypanosomosis in clinically healthy cattle of north Cameroon: Epidemiological implications. Parasites and Vectors *9*, 206.

Maxie, M.G., and Losos, G.J. (1977). Release of *Trypanosoma congolense* from the microcirculation of cattle by Berenil. Vet. Parasitol. *3*, 277–281.

May, M.J., and Ager, A. (1992). ICAM-1-independent lymphocyte transmigration across high endothelium : Differential up-regulation by interferon γ, tumor necrosis factor-α and interleukin 1β. Eur. J. Immunol. *22*, 219–226.

McCarthy, D.J., Chen, Y., and Smyth, G.K. (2012). Differential expression analysis of multifactor RNA-Seq experiments with respect to biological variation. Nucleic Acids Res.

Medana, I.M., and Turner, G.D.H. (2006). Human cerebral malaria and the blood-brain barrier. Int. J. Parasitol. *36*, 555–568.

Medoff, B.D., Wain, J.C., Seung, E., Jackobek, R., Means, T.K., Ginns, L.C., Farber, J.M., and Luster, A.D. (2005). Function of Obliterative Bronchiolitis: Regulation and CXCR3 and Its Ligands in a Murine Model. J. Immunol. *176*, 7087–7095.

Michlmayr, D., and Mckimmie, C.S. (2014). Role of CXCL10 in central nervous system inflammation. Int. J. Interf. Cytokine Mediat. Res. *6*.

Morawski, P.A., Qi, C.F., and Bolland, S. (2017). Non-pathogenic tissue-resident CD8+ T cells uniquely accumulate in the brains of lupus-prone mice. Sci. Rep. *7*, 1–13.

De Niz, M., Nacer, A., and Frischknecht, F. (2019a). Intravital microscopy: Imaging host-parasite interactions in the brain. Cell. Microbiol. *2019*, e13024.

De Niz, M., Meehan, G.R., Brancucci, N.M.B., Marti, M., Rotureau, B., Figueiredo, L.M., and Frischknecht, F. (2019b). Intravital imaging of host-parasite interactions in skin and adipose tissues. Cell. Microbiol. *21*, 13023.

De Niz, M., Carvalho, T., Carlos Penha-Gonçalves, and Agop-Nersesian, C. (2020). Intravital imaging of host-parasite interactions in organs of the thoracic and abdominopelvic cavities. Cell. Microbiol. *22*, e13201.

De Niz, M., Brás, D., Ouarné, M., Pedro, M., Nascimento, A.M., Misikova, L.H., Franco, C.A., and Figueiredo, L.M. (2021). Organotypic endothelial adhesion molecules are key for *Trypanosoma brucei* tropism and virulence. Cell Rep. *36*, 109741.

Noyes, H.A., Alimohammadian, M.H., Agaba, M., Brass, A., Fuchs, H., Gailus-Durner, V., Hulme, H., Iraqi, F., Kemp, S., Rathkolb, B., et al. (2009). Mechanisms controlling anaemia in *Trypanosoma congolense* infected mice. PLoS One *4*.

Pertea, M., Pertea, G.M., Antonescu, C.M., Chang, T.C., Mendell, J.T., and Salzberg, S.L. (2015). StringTie enables improved reconstruction of a transcriptome from RNA-seq reads. Nat. Biotechnol.

Robinson, M.D., McCarthy, D.J., and Smyth, G.K. (2010). edgeR: a Bioconductor package for differential expression analysis of digital gene expression data. Bioinformatics.

Rogers, D.C., Fisher, E.M.C., Brown, S.D.M., Peters, J., Hunter, A.J., and Martin, J.E. (1997). Behavioral and functional analysis of mouse phenotype: SHIRPA, a proposed protocol for comprehensive phenotype assessment. Mamm. Genome *8*, 711–713.

Rogerson, S.J., Hviid, L., Duffy, P.E., Leke, R.F., and Taylor, D.W. (2007). Malaria in pregnancy: pathogenesis and immunity. Lancet Infect. Dis. *7*, 105–117.

Sancho, D., Yáñez-Mó, M., Tejedor, R., and Sánchez-Madrid, F. (1999). Activation of peripheral blood T cells by interaction and migration through endothelium: Role of lymphocyte function antigen-1/intercellular adhesion molecule-1 and interleukin-15. Blood *93*, 886–896.

Sanz, E., Yang, L., Su, T., Morris, D.R., McKnight, G.S., and Amieux, P.S. (2009). Cell-type-specific isolation of ribosome-associated mRNA from complex tissues. Proc. Natl. Acad. Sci. U. S. A. *106*, 13939–13944.

Savage, V.L., Christley, R., Pinchbeck, G., Morrison, L.J., Hodgkinson, J., and Peachey, L.E. (2021). Co-infection with *Trypanosoma congolense* and *Trypanosoma brucei* is a significant risk factor for cerebral trypanosomosis in the equid population of the Gambia. Prev. Vet. Med. *197*, 105507.

Schumak, B., Klocke, K., Kuepper, J.M., Biswas, A., Djie-Maletz, A., Limmer, A., van Rooijen, N., Mack, M., Hoerauf, A., and Rita Dunay, I. (2015). Specific Depletion of Ly6C hi Inflammatory Monocytes Prevents Immunopathology in Experimental Cerebral Malaria. PLoS One *10*, e0124080.

Silva Pereira, S., Trindade, S., De Niz, M., and Figueiredo, L.M. (2019). Tissue tropism in parasitic diseases. Open Biol. *9*, 190036.

Smyth, G.K., Ritchie, M.E., Law, C.W., Alhamdoosh, M., Su, S., Dong, X., and Tian, L. (2018). RNA-seq analysis is easy as 1-2-3 with limma, Glimma and edgeR. F1000Research *5*, 1–30.

Sondgeroth, K.S., Mcelwain, T.F., Allen, A.J., Chen, A. V, and Lau, A.O. (2013). Loss of neurovirulence is associated with reduction of cerebral capillary sequestration during acute *Babesia bovis* infection. Parasit. Vectors *6*, 181.

Sorensen, E.W., Lian, J., Ozga, A.J., Miyabe, Y., Ji, S.W., Bromley, S.K., Mempel, T.R., and Luster, A.D. (2018). CXCL10 stabilizes T cell-brain endothelial cell adhesion leading to the induction of cerebral malaria. JCI Insight *3*.

Van den Steen, P.E., Deroost, K., Deckers, J., Van Herck, E., Struyf, S., and Opdenakker, G. (2013). Pathogenesis of malaria-associated acute respiratory distress syndrome. Trends Parasitol. *29*, 346–358.

Stijlemans, B., Beschin, A., Magez, S., Van Ginderachter, J.A., and De Baetselier, P. (2015). Iron Homeostasis and *Trypanosoma brucei* Associated Immunopathogenicity Development: A Battle/Quest for Iron. Biomed Res. Int. 819389.

Storm, J., and Craig, A.G. (2014). Pathogenesis of cerebral malaria - inflammation and cytoadherence. Front. Cell. Infect. Microbiol. *4*, 100.

Subramanian, A., Tamayo, P., Mootha, V.K., Mukherjee, S., Ebert, B.L., Gillette, M.A., Paulovich, A., Pomeroy, S.L., Golub, T.R., Lander, E.S., et al. (2005). Gene set enrichment analysis: A knowledge-based approach for interpreting genome-wide expression profiles. Proc. Natl. Acad. Sci. *102*, 15545–15550.

Tripathi, A.K., Sullivan, D.J., and Stins, M.F. (2006). *Plasmodium falciparum*-infected erythrocytes increase intercellular adhesion molecule 1 expression on brain endothelium through NF-κB. Infect. Immun. *74*, 3262–3270.

Wang, J., Vasaikar, S., Shi, Z., Greer, M., and Zhang, B. (2017). WebGestalt 2017: a more comprehensive, powerful, flexible and interactive gene set enrichment analysis toolkit. Nucleic Acids Res. *45*, W130–W137.

Yipp, B.G., Anand, S., Schollaardt, T., Patel, K.D., Looareesuwan, S., and Ho, M. (2000). Synergism of multiple adhesion molecules in mediating cytoadherence of *Plasmodium falciparum*-infected erythrocytes to microvascular endothelial cells under flow. Blood *96*, 2292–2298.

Young, C.J., and Godfrey, D.G. (1983). Enzyme polymorphism and the distribution of *Trypanosoma congolense* isolates. Ann. Trop. Med. Parasitol. *77*, 467–481.

Figures

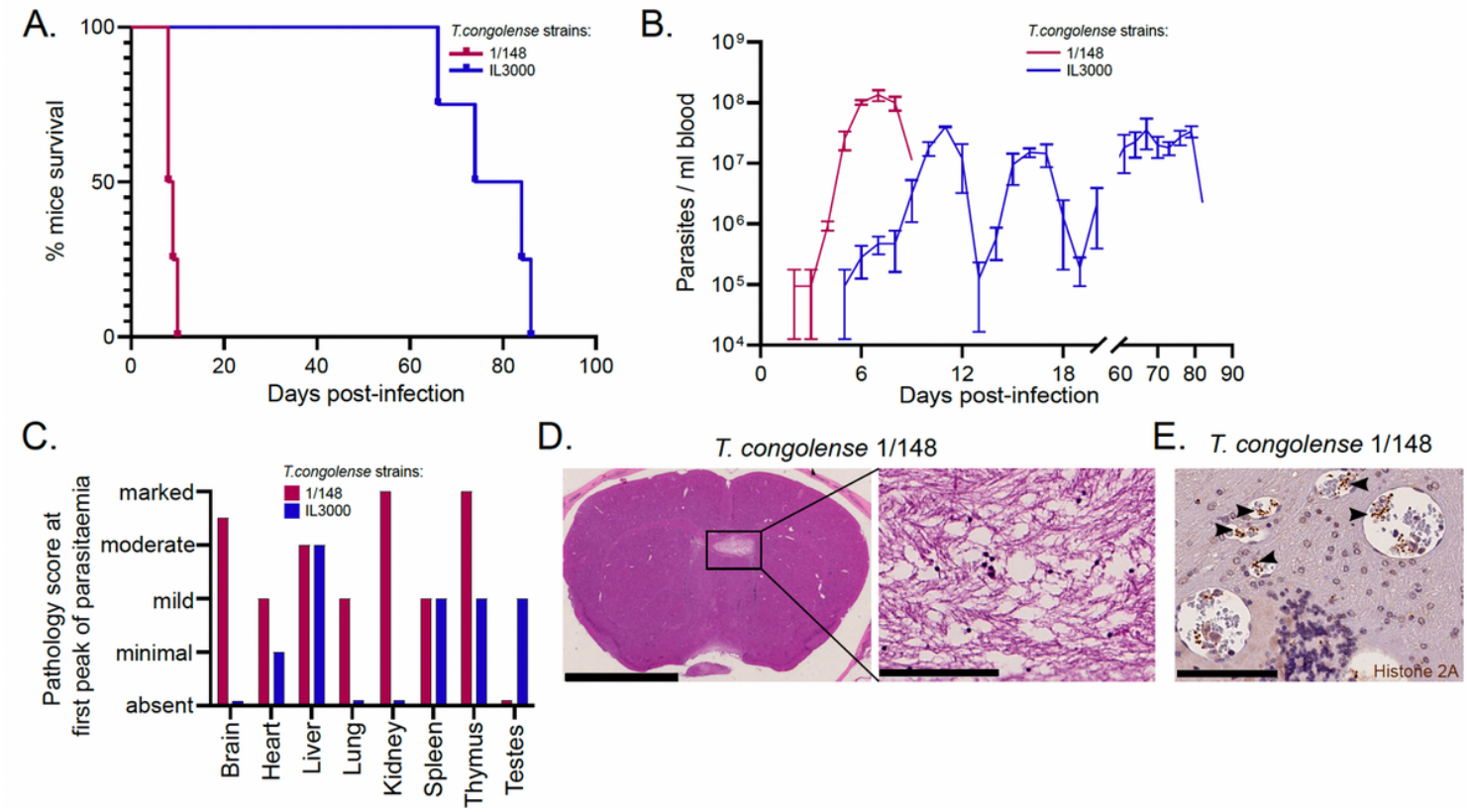

Figure 1

Infection progression and phenotypic differences between T. congolense savannah strains IL3000 (12) and 1/148 (13). A. Mice survival curves following infection with T. congolense strains 1/148 and IL3000 (average of 9.0±0.4 and 77.5±4.0 (Mean ± SEM) days respectively) (N = 4). B. Parasitaemia throughout infection with 1/148 and IL3000 parasites estimated by hemocytometry shows that infections with strain 1/148 do not progress past the first peak of parasitaemia, whereas parasitaemia with strain IL3000 oscillates from below the level of detection to 5x107 parasites/ml for up to 84 days. C. Pathological report at the first peak of parasitaemia of each strain, scored based on the degree of organ damage from absent to marked. D. Right: Representative histological hematoxylin & eosin staining of brain of a mouse infected with strain 1/148, showing a large lesion (Scale bar = 2.5 mm). Right: high-magnification of lesion, showing cell loss (scale bar = 100 µm) E. Immuno-histochemical staining of trypanosome H2A (brown), showing parasite sequestration in the brain vasculature. Scale bar = 100 µm

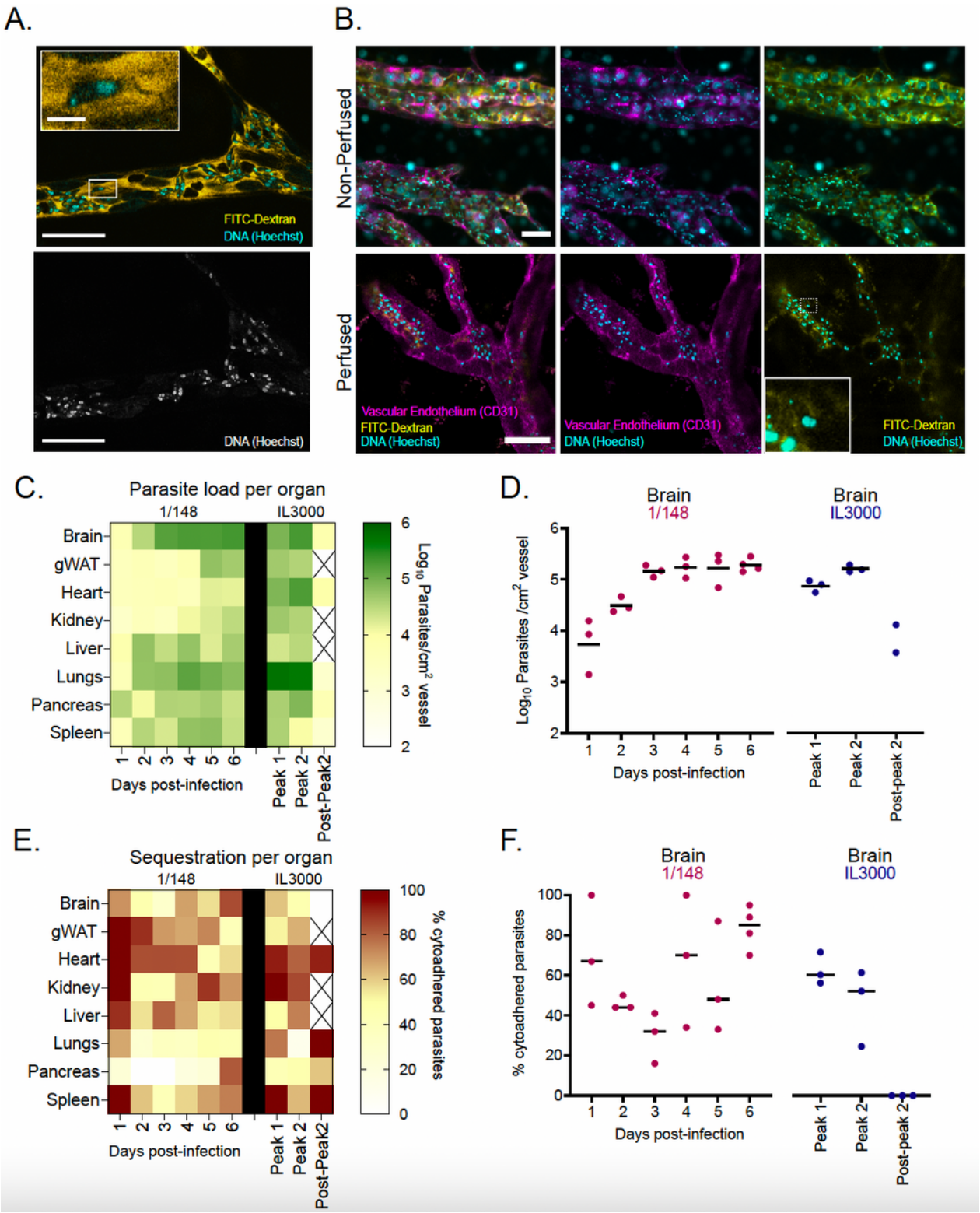

Figure 2

Trypanosoma congolense sequestration depends on the strain and tissue, but not on parasite load. A. Representative image of T. congolense parasites in a vessel of the brain by intravital microscopy at day 6 post-infection. 70 kDa FITC-Dextran is used for vascular flow labeling (shown in yellow); cell nuclei are stained with Hoechst (shown in cyan). Bottom panel shows nuclei staining only. Scale = 20 µm. On top-left, a zoomed-in section showing a T. congolense parasite. Scale = 4 µm. B. Representative images of T.

congolense parasites in brain vessels by intravital microscopy at day 6 post-infection, without (top) and with (bottom) perfusion. 70 kDa FITC-Dextran is used for vascular flow labeling (shown in yellow); cell nuclei are stained with Hoechst (shown in cyan), vascular endothelium is stained with α-A637-CD31. Scale = 30 µm. On bottom-right, a zoomed-in section showing a cytoadhered T. congolense parasite after perfusion. C. Heatmap showing total parasite load per organ over the course of the infection in strains 1/148 and IL3000, quantified by intravital microscopy and represented as log2 parasites per cm2 of vessel, adjusted for the vascular density of each organ. D. Total parasite load in the brain vasculature over the course of the infection in strains 1/148 and IL3000, quantified by intravital microscopy. E. Heatmap showing percentage of cytoadhered parasites per organ over the course of the infection in strains 1/148 and IL3000, quantified by intravital microscopy. F. Percentage of cytoadhered parasites in the brain vasculature over the course of the infection in strains 1/148 and IL3000, quantified by intravital microscopy. Black line indicates geometric mean for parasite load and median for sequestration percentage. Strains are color-coded according to key. N = 3, 3 independent infections.

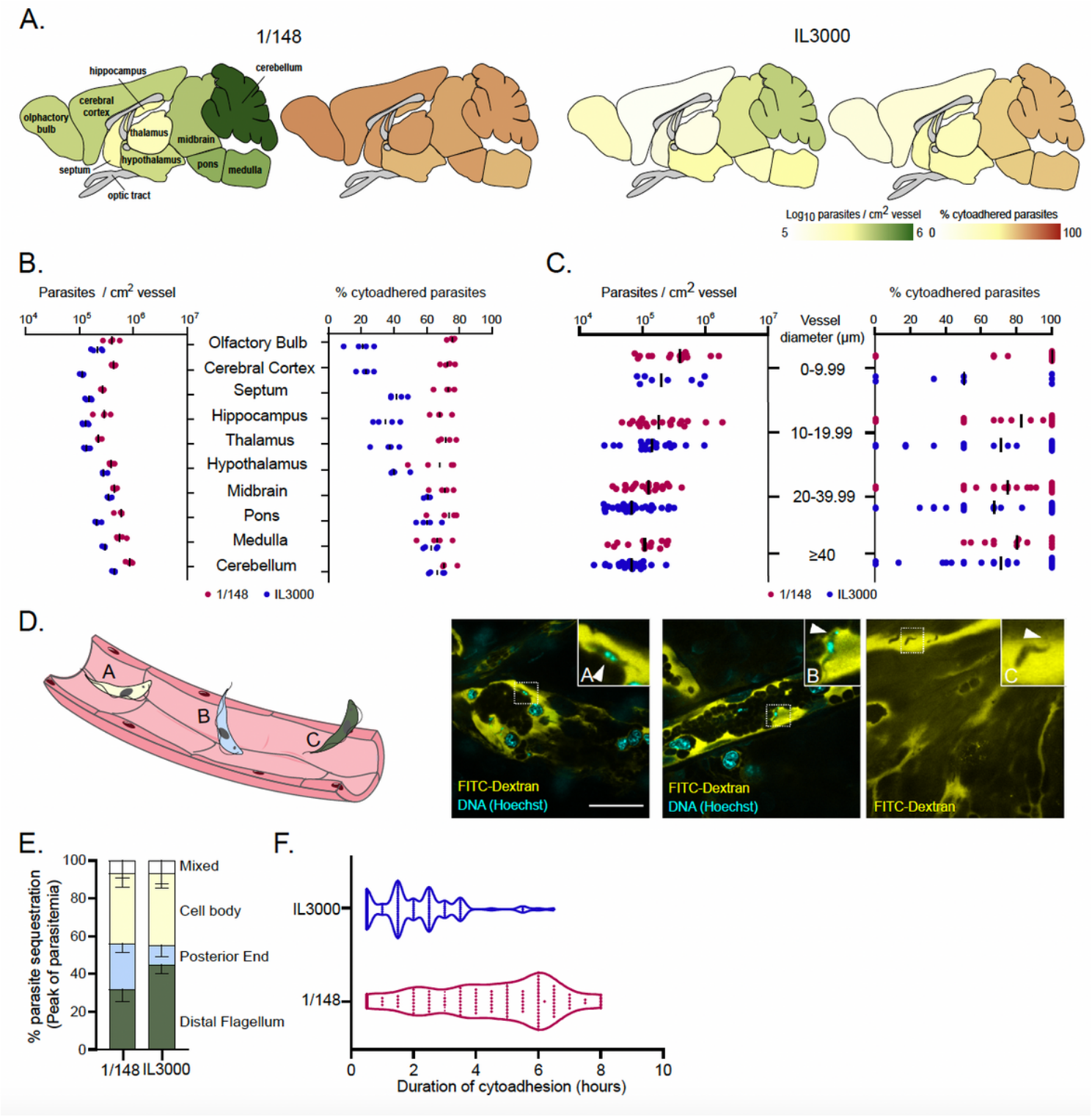

Figure 3

Distribution and characterization of Trypanosoma congolense sequestration in the brain. A. Total parasite load (green) and percentage of parasite sequestration (orange) in different parts of the brain at the first peak of parasitaemia of strains 1/148 and IL3000, quantified by ex-vivo microscopy in a minimum of 100 separate images in 3-4 separate mice. B. Quantitative values corresponding to (A) at the first peak of parasitaemia. C. Parasite load (left) and sequestration proportion (right) in vessels of

different diameters. D. Illustrative cartoon depicting the different parts of the parasite that can adhere to the endothelium, namely (A) cell body, (B) posterior end and (C) distal flagellum, and three representative images obtained by intravital microscopy at day 6 post-infection. 70 kDa FITC-Dextran is used for vascular flow labeling (shown in yellow); cell nuclei are stained with Hoechst (shown in cyan). Scale = 30 µm. E. Characterization of the cytoadhered population in the brain (displayed as percentage) of strains 1/148 and IL3000, based on which part of the cell adheres to the endothelial cell. Mixed means that parasites attached with more than one part of the cell during a single video acquisition. Mean ± SD. F. Time (in hours) that individual parasites remain cytoadhered. Images were obtained every 30 minutes, for 12 hours. Black line indicates mean. N = 3, 3 independent infections, 100 vessels per mouse.

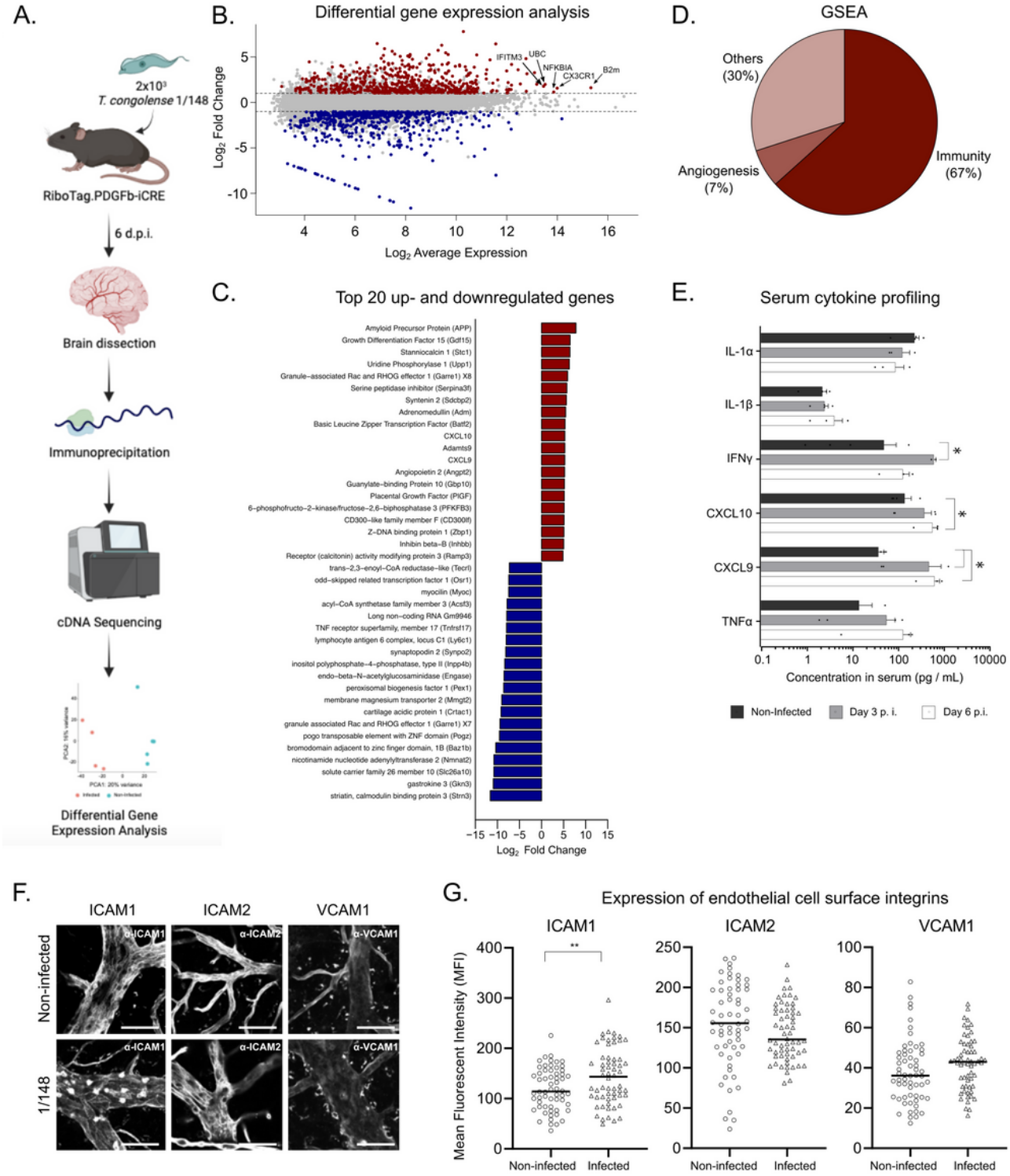

Figure 4

Parasite presence induces a pro-inflammatory profile in brain endothelial cells. A. Schematics of the methodology used to compare the transcriptomes of brain endothelial cells. RiboTag.PDGFb.iCRE mice, under Cre recombinase induction, were infected with 2x103 T. congolense 1/148 parasites intra-peritoneally. At day 6 post-infection, mice were euthanized, perfused and brains were dissected and homogenized. The polysomes of endothelial cells were immunoprecipitated and the RNA extracted and

converted into cDNA, which was sequenced on a NextSeq 500 platform as 75bp single-end reads (N = 4-5). Figure created with BioRender.com. B. Distribution of detected transcripts in terms of average expression and fold change between infected and non-infected conditions. Transcripts upregulated in infection are shown in red (N = 612), downregulated transcripts are shown in blue (N = 588). The top most abundant upregulated transcripts are identified: beta-2 microglobulin (B2m), chemokine (C-X3-C motif) receptor 1 (Cx3cr1), nuclear factor of kappa light polypeptide gene enhancer in B cells inhibitor, alpha (Nfkbia), ubiquitin C (UBC), and interferon induced transmembrane protein 3 (Ifitm3). C. The 20 most up- and downregulated transcripts detected upon infection, ordered by Log2 fold change. D. Enriched gene sets upon infection (FDR< 0.05) detected by gene ontology-based gene set enrichment analysis (Subramanian et al., 2005), produced by WEBgestalt (Wang et al., 2017), and ordered by the normalized enriched score. E. Serum concentration of IL-1α, IL-1β, IFNγ, CXCL10, CXCL9, TNFα in non-infected mice and at days 3 and 6 post-infection (N = 3-4). F. Representative images of ICAM1, ICAM2, and VCAM1 expression in the brain endothelium of non-infected and infected mice, measured by fluorescence. G. Mean fluorescent intensity of ICAM1, ICAM2, and VCAM in the brain endothelium in non-infected mice and in mice infected with T. congolense 1/148, at day 6 post-infection. Black lines represent mean. Stars indicate statistically significant results; unpaired t-test, * $p < 0.05$; ** $p < 0.01$; *** $p < 0.001$; **** $p < 0.0001$.

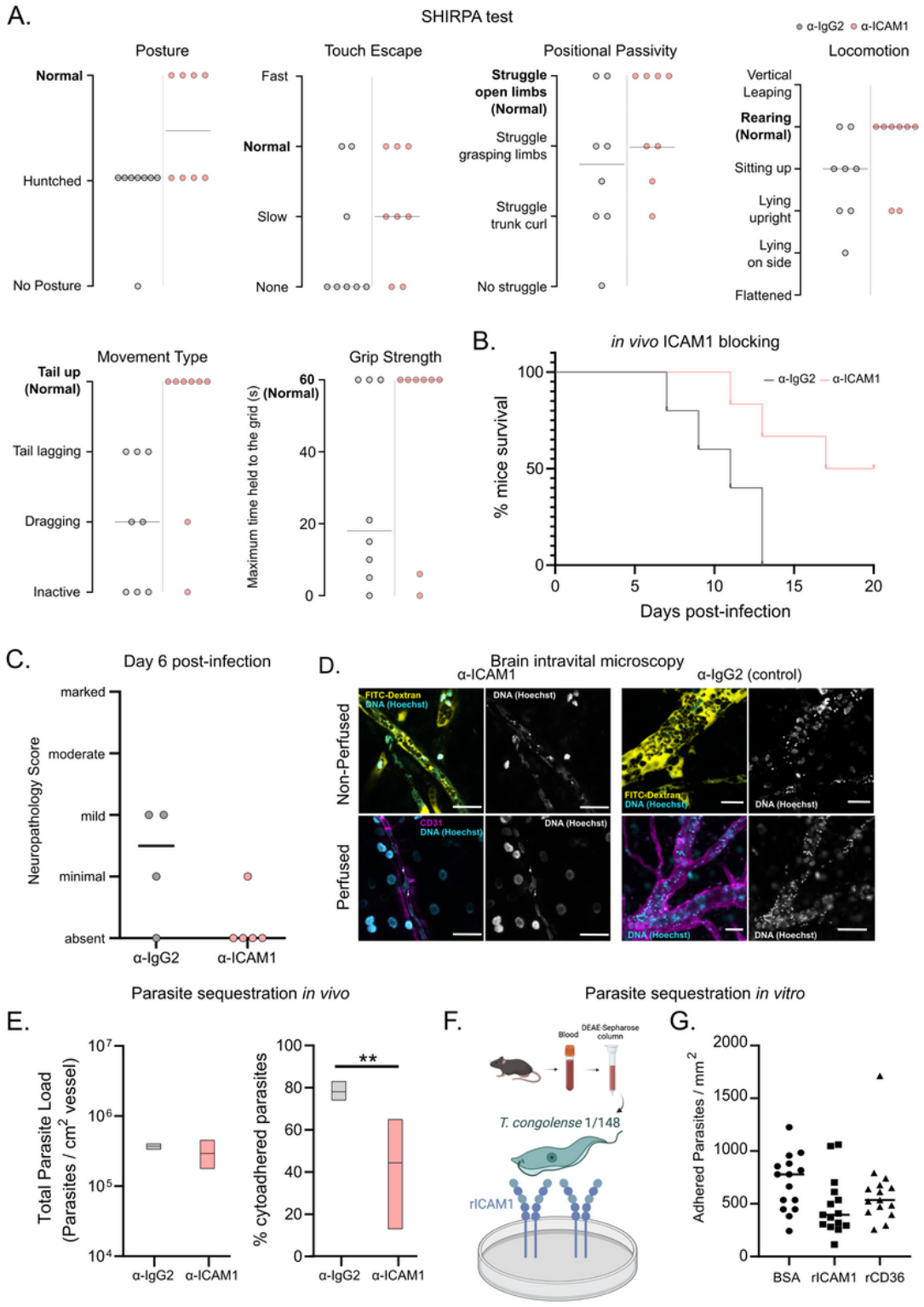

Figure 5

Phenotypic effects of α-ICAM1 antibody treatment in mice infected with T. congolense 1/148. A. Behavioral assessment of mice treated with either α-ICAM1 antibody or its isotype control (α-IgG2), based on the SHIRPA protocol. The parameters assessed and shown are: Posture, Touch Escape, Positional Passivity, Locomotion, Movement Type (and tail posture), and Grip Strength: Time (in seconds) that mice can hold upside down on a grid (maximum of 1 minute). Black line indicates median. B. Mice survival

curves following treatment with α-ICAM1 antibody (α-ICAM1) or its isotype control (α-IgG2). Results were pooled from two independent experiments (N = 6). C. Neuropathology score at day 6 post-infection of mice infected with T. congolense 1/148, treated with α-CAM1 antibody or its isotype control (N = 4-5). Black line indicates median. D. Representative images obtained by intravital microscopy, of parasite sequestration in the brain vasculature upon treatment with α-ICAM1 antibody or its isotype control (α-IgG2) with and without perfusion, at day 6 post-infection. Scale bar = 30 µm. E. Parasite load (left) and percentage of parasite sequestration (right) in the brain of mice at day 6 post-infection upon treatment with α-ICAM1 antibody or its isotype control (α-IgG2), quantified by intravital microscopy (N = 3 in 3 independent infections). Stars indicate statistically significant results; mixed models, ANOVA, multiple comparisons test, * $p < 0.05$; ** $p < 0.01$; *** $p < 0.001$; **** $p < 0.0001$. F. Schematics of in vitro recombinant ICAM1 binding assay used to assess parasite sequestration in vitro. T. congolense 1/148 parasites in blood were collected from a donor mouse and separated from the blood by anion exchange chromatography on a DEAE-sepharose column. Parasites were added to culture plates previously coated with recombinant ICAM1 and parasite binding was assessed by microscopy. G. Quantification of parasite binding to bovine serum albumin (blocking protein), recombinant ICAM1 (rICAM1), or recombinant CD36 (rCD36) (negative control). Black line indicates mean.

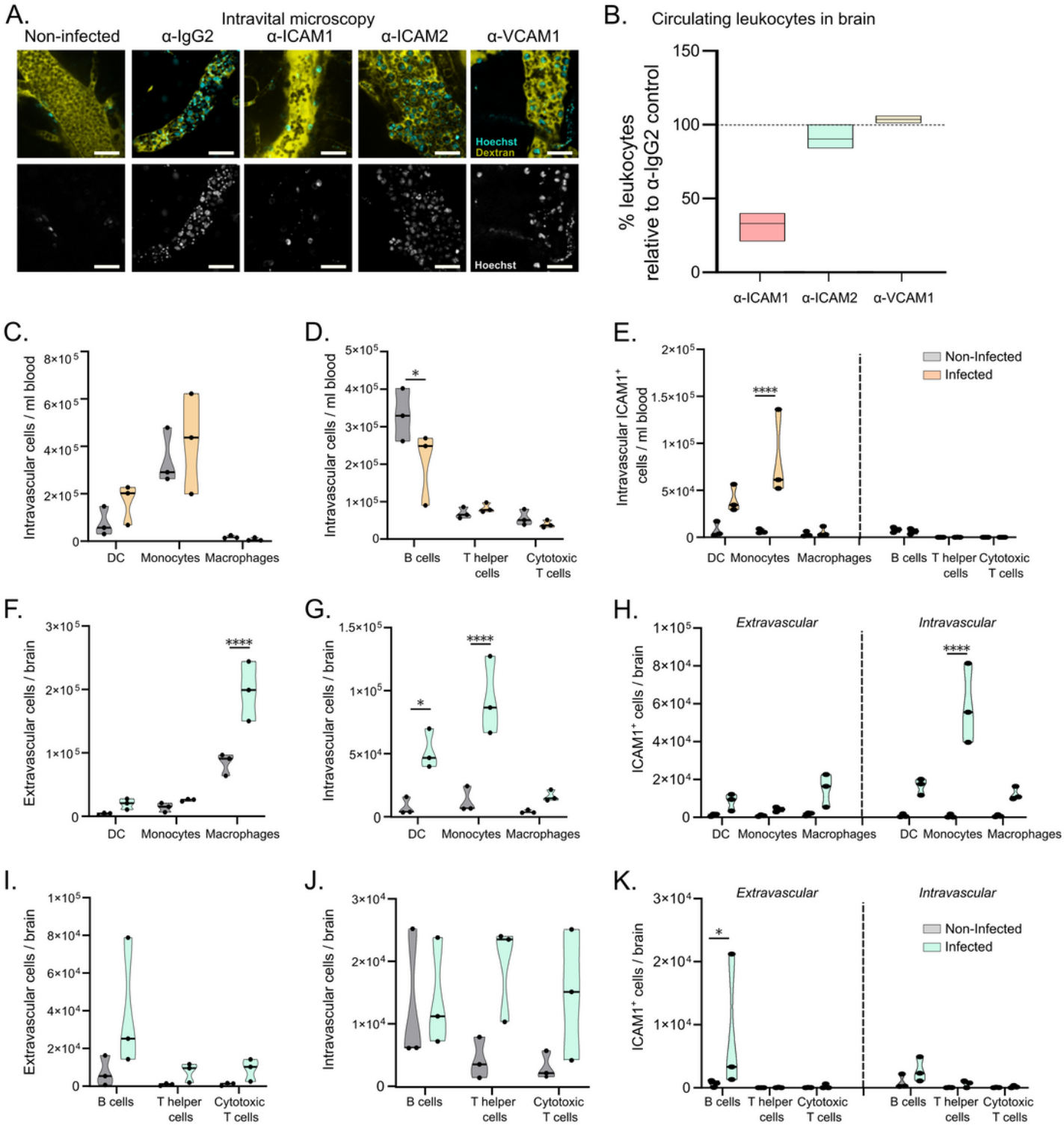

Figure 6

Characterization of immune cell populations infiltrating and circulating in the brain and systemic vasculature at day 6 post-infection with T. congolense 1/148. A. Representative images obtained by intravital microscopy, of leukocytes in the brain vasculature in non-infected mice, and mice infected with T. congolense 1/148, but treated with antibodies against IgG2 (isotype control), ICAM1, ICAM2, or VCAM1. Nuclei are stained with Hoechst dye and shown in green. B. Percentage of leukocytes found in the brain

vasculature at day 6 post-infection in mice treated with α-ICAM1, α-ICAM2, or α-VCAM1, relative to the isotype control (represented as 100%). Black line indicates mean. (N = 3 in 3 independent infections). C. Number of myeloid cells (CD11b+) per mL of blood, separated by cell type (CD11c+ Dendritic Cells, Ly6C+ Monocytes, and F4/80 Macrophages) in non-infected and infected mice. D. Number of non-myeloid (CD11b-) cells per mL of blood, separated by cell type (CD19+ B cells, CD3+CD4+ T cells, CD3+CD8+ T cells) in non-infected and infected mice. E. Number of leukocytes (CD45+) expressing ICAM1 per mL of blood, separated by cell type, in non-infected and infected mice. F. Number of extravascular (APC:CD45-) myeloid (CD11b+) cells per brain of mice, separated by cell type in non-infected and infected mice. G. Number of intravascular (APC:CD45+) myeloid (CD11b+) cells per brain of mice, separated by cell type, in non-infected and infected mice. H. Number of extravascular (APC:CD45-) and intravascular (APC:CD45+) myeloid (CD11b+) cells expressing ICAM1 per brain of mice, separated by cell type, in non-infected and infected mice. I. Number of extravascular (APC:CD45-) non-myeloid (CD11b-) cells per brain of mice, separated by cell type in non-infected and infected mice. G. Number of intravascular (APC:CD45+) non-myeloid (CD11b-) cells per brain of mice, separated by cell type, in non-infected and infected mice. H. Number of extravascular (APC:CD45-) and intravascular (APC:CD45+) non-myeloid (CD11b-) cells expressing ICAM1 per brain of mice, separated by cell type, in non-infected and infected mice. Stars indicate statistically significant results; unpaired t-test, * $p < 0.05$; ** $p < 0.01$; *** $p < 0.001$; **** $p < 0.0001$. Black line indicates mean. N = 3.

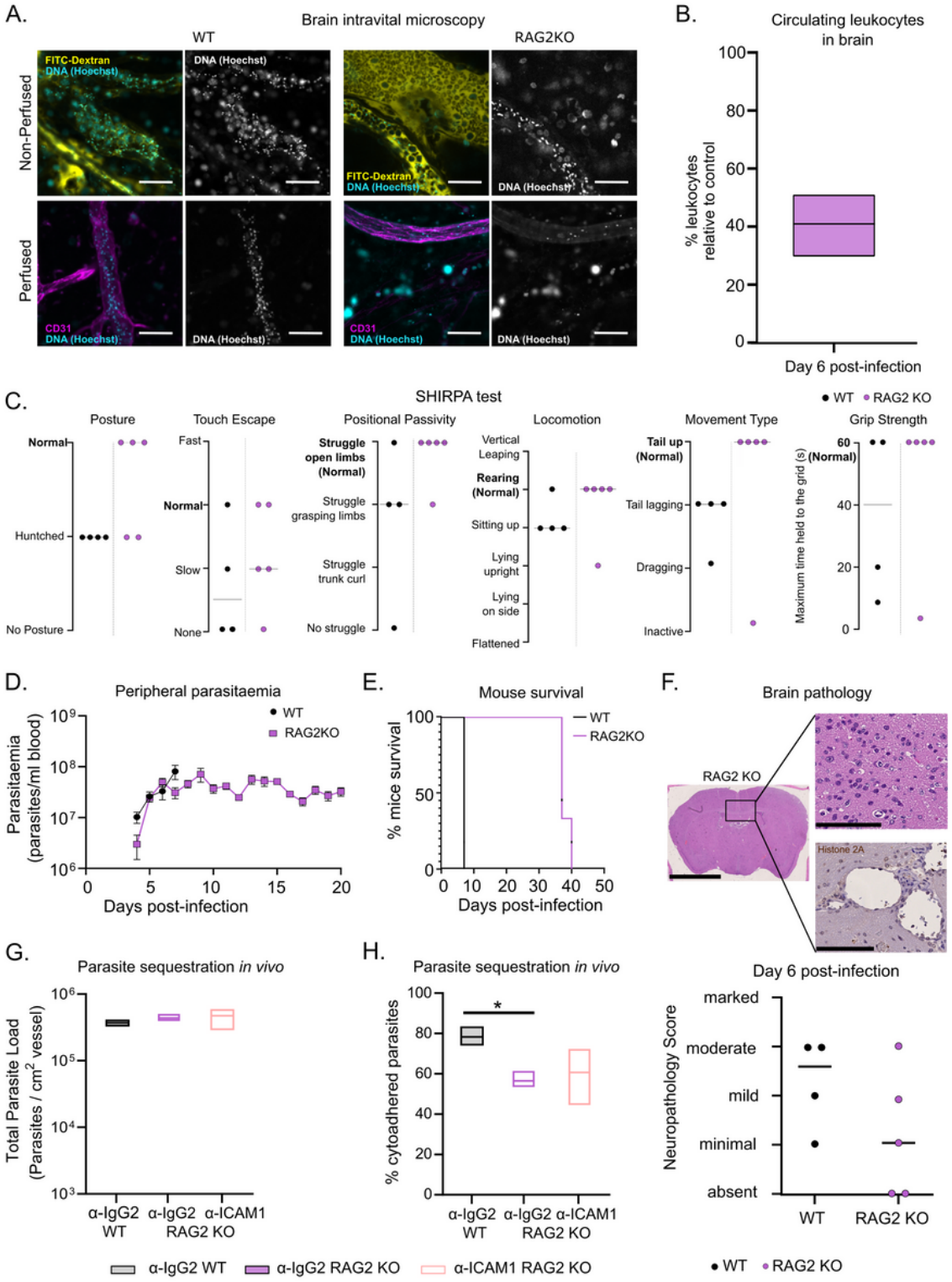

Figure 7

T. congolense 1/148 sequestration load and infection progression in RAG2 KO mice. A. Representative images of parasite sequestration in brains of WT and RAG2 KO mice with and without perfusion, at day 6 post-infection. Scale bar = 30 µm. B. Percentage of leukocytes found in the brain vasculature at day 6 post-infection in RAG2 KO mice relative to WT control. C. Behavioral assessment of mice treated with either a-ICAM1 antibody or its isotype control (a-IgG2), based on the SHIRPA protocol. Black line indicates

median. D. Parasitaemia curve of T. congolense 1/148 in WT or RAG2 KO mice, measured by hemocytometry. E. Mice survival curves of WT and RAG2 KO mice (N = 4). F. Top: Neuropathology score at day 6 post-infection of RAG2 KO and WT mice infected with T. congolense 1/148 (N = 4-5). Black line indicates median. Bottom right: Representative histological hematoxylin & eosin staining of brain of a RAG2 KO mouse infected with strain 1/148, showing absence of lesions in the brain parenchyma (Scale bar = 2.5mm). Top right: high-magnification of brain parenchyma (scale bar = 100 µm). Bottom right: Immuno-histochemical staining of trypanosome histone 2A (brown) showing little parasite sequestration in the brain vasculature. Scale bar = 100 µm. G. Parasite load in the brain of WT or RAG2 KO mice, treated with either α-IgG2 or α-ICAM1 antibody, quantified by intravital microscopy, at day 6 post-infection. H. Percentage of cytoadhered parasites in the brain of WT or RAG2 KO mice, treated with either α-IgG2 or α-ICAM1 antibody, quantified by intravital microscopy. Stars indicate statistically significant results; 2-way ANOVA, multiple comparisons test, * $p < 0.05$; ** $p < 0.01$; *** $p < 0.001$; **** $p < 0.0001$. (N = 3 in 3 independent infections).

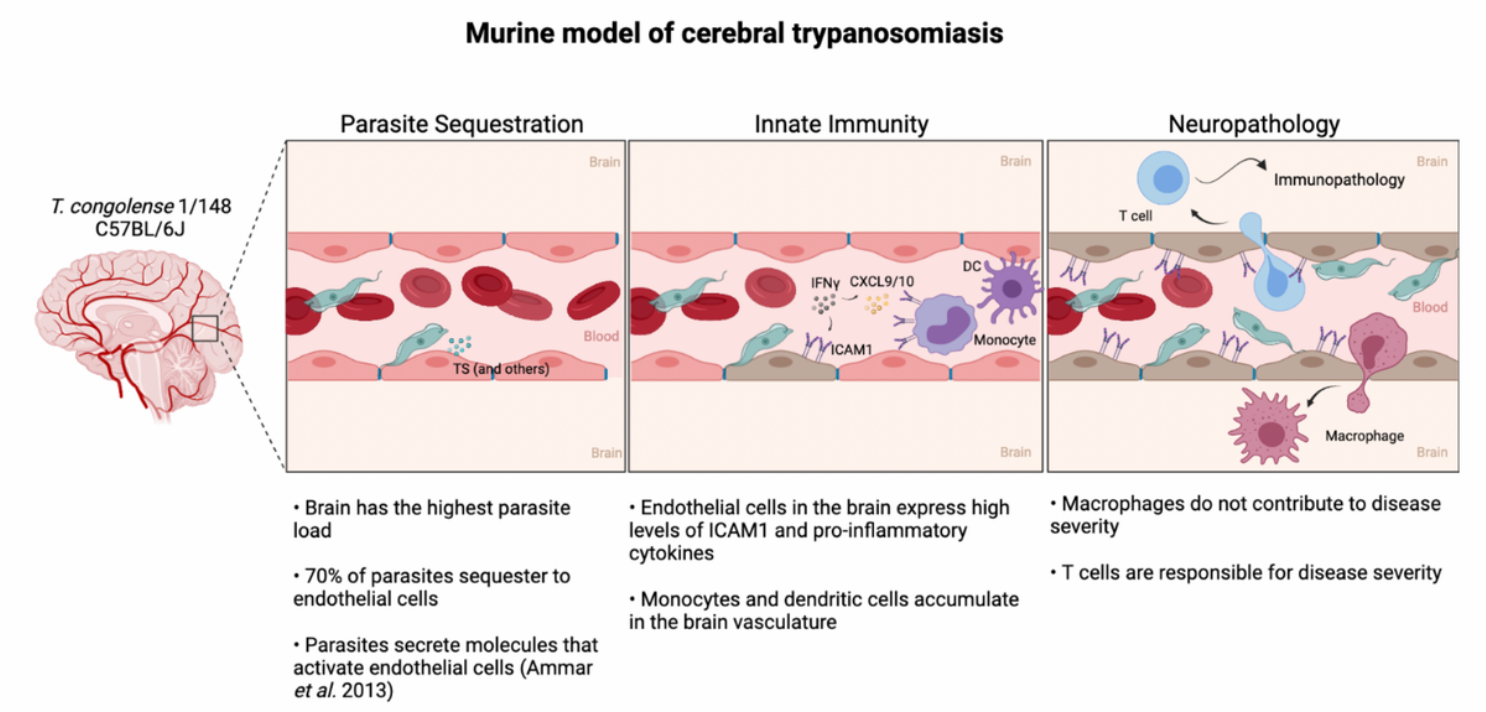

Figure 8

Murine model of cerebral animal African trypanosomiasis. Upon infection of C57BL/6J mice with T. congolense 1/148 parasites cytoadhere to the brain vasculature (“Parasite Sequestration”). The physical damage caused by sequestration and the release of parasitic molecules, like trans-sialidases, activates the endothelium leading to an increase in expression and secretion of pro-inflammatory molecules (e.g. ICAM1, IFNγ, CXCL9, CXCL10), as well as the recruitment of innate cells (i.e. DC, monocytes) (“Innate Immunity”). Innate cells and activated endothelial cells recruit T cells to the brain vasculature and promote monocyte differentiation into inflammatory macrophages. Both T cells and inflammatory macrophages cross the blood-brain-barrier and infiltrate the brain parenchyma, but T cells cause the neuropathology associated with acute disease (“Neuropathology”). Figure created with BioRender.com.

Supplementary Files

This is a list of supplementary files associated with this preprint. Click to download.

- SFig1.pdf
- SFig2.pdf
- SFig2.pdf
- SFig4.pdf
- SFig5.pdf
- SVideo1.avi
- SVideo2.avi
- SVideo3.avi
- SVideo4.avi
- SVideo5.avi
- SupTable1.xlsx
- SupTable2.xlsx